First of all, we thank Ray Nassar (reviewer 1) for his efforts in carefully reviewing our manuscript and his constructive comments.

Point-by-point answers to the comments of reviewer 1

Specific points

Reviewer 1: *Page 2, lines 15-17 is a jumble of references to different techniques and different types of measurements (satellites and airborne). Since the rest of the paper is about satellite observations, the reference to the airborne measurements and associated emission estimates of Krings et al. 2011 and 2018 should either be removed or some explanation is needed as to why they are relevant here.*
Authors: We cited the publications of Krings et al. (2011, 2018) as examples where assumptions on source position and plume formation have been made. However, as they are not analyzing satellite measurements, we removed them from the revised manuscript.

Reviewer 1: *It would also be useful to better distinguish between studies that quantified/estimated emissions versus identification.*
Authors: In the revised version, we cite only studies related to quantification/estimation of emissions which is more appropriate in this context: "... and the quantification of anthropogenic emissions a challenging task. Usually, the latter requires knowledge of the source position and assumptions on plume formation (e.g., Nassar et al., 2017; Heymann et al., 2017) or statistical approaches applied on larger areas and/or time periods (e.g., Schneising et al., 2013; Buchwitz et al., 2017)."

Reviewer 1: *It might also be helpful to point out the studies that took advantage of atmospheric imaging capability, which is crucial to the current work.*
Authors: Here we are aiming to directly lead to emission estimates which make use of simultaneous NO_2 measurements. The benefits of imaging capabilities are discussed at p15 l16 of the original manuscript.

Reviewer 1: *P2, L27. Specifying that the S5P launch was in October 2017 would help to clarify for the reader why only observations from 2018 were used in this work.*
Authors: Done.

Reviewer 1: *P3, L8: "eight parallelogram-shaped footprints across track with a spatial resolution at ground of <= 1.29 km x 2.25 km"*
Authors: Done.

Reviewer 1: *P3, L13: It would be helpful to add a statement along*

the lines of "The OCO-2 v9 data set has an improved bias correction approach that results in reduced biases particularly over areas of rough topography."
Authors: Done.

Reviewer 1: *P4, L2: It would be helpful to provide the SNR or perhaps a relative precision instead of just the random noise, since most CO2 specialists will not have a good grasp of the magnitude with these units.*
Authors: We added: "(enhancements near sources often exceed 10^{16} molec./cm^2)".

Reviewer 1: *P4, L14: "50 minutes" According to the figure labels, the time differences range from 6 minutes (Medupi-Matimba) to 35 minutes (Nanjing). Perhaps it would be more informative to state: "each scene observed by OCO-2 is also observed by S5P with a temporal offset ranging from 6 to 35 minutes"?*
Authors: About 50 minutes is the maximum co-location time difference for the vast majority of possible OCO-2 observations. 6 to 35 minutes is only the range for the presented cases (which are described later in the paper).

Reviewer 1: *P5, L5-10: The method described is interesting and very sensible and is one of the strengths of this work.*
Authors: Many thanks.

Reviewer 1: *P5, L29 – P6 L1: The manual adjustment to wind direction but not windspeed is similar to the approach of Nassar et al. (2017) which would be worth acknowledging.*
Authors: We added: "The manual adjustment to wind direction but not wind speed is similar to the approaches of, e.g., Krings et al. (2011) or Nassar et al. (2017)."

Reviewer 1: *P6, L7: This constant factor of 1.44 taken from Varon et al. (2018) to treat the vertical dimension is a major oversimplification in this work. Varon et al. (2018) simulated CH4 plumes that might be typical of CH4 leaks from infrastructure, thus they deal with smaller spatial scales and little to no temperature contrast. The effective vertical height of emissions will likely be very different when dealing with smokestacks, urban areas or wildfires, as in the present work. In fact, a new paper (Brunner et al. "Accounting for the vertical distribution of emissions in atmospheric CO2 simulations" Atmos. Chem. Phys., https://doi.org/10.5194/acp-19-4541-2019) that also has links to the Copernicus candidate CO2 Monitoring mission, describes the relevant factors for the vertical distribution of emissions, where different vertical emission profiles for point sources (i.e. a power plant) or area sources (i.e. an urban area) are discussed. The temperature of the emissions and the season are also shown to be important factors. Although detailed study of plume rise is complex and beyond the scope of this paper, and the use of column data reduces the importance of these issues, surely it must be too simple to use a single factor of*

1.44 times the 10 m wind speed to represent plume rise from the diversity of source types and geographic locations studied in the present work. According to equation 3, errors in emission estimates will be approximately proportional to the error in wind speed, so getting a realistic wind speed is important.
Authors: As discussed at p6 l9, the focus of our study is "on demonstrating the benefits of simultaneous NO_2 and XCO_2 measurements rather than on most accurate flux estimates" and we "recognize that uncertainties resulting from our estimate of the effective wind speed's normal may be reduced in the future by improved wind knowledge". At p6 l26, we acknowledge the differences of our study compared to the study of Varon et al. (2018) and account this by enhancing the introduced uncertainty. Within the revised version of the manuscript, we cite Brunner et al. (2019) and the paragraph starting at p6 l5 now reads: "As discussed by Brunner et al. (2019), the plume height (and subsequently the wind speed in plume height) depends on many aspects like emission height, stack geometry, flue gas exit velocity and temperature, meteorological conditions, etc. Some of these parameters are not known for many sources and their explicit consideration would go beyond the scope of this study focusing on demonstrating the benefits of simultaneous NO_2 and XCO_2 measurements rather than on most accurate flux estimates. Varon et al. (2018) proposed to approximate the effective wind speed within the plume from the 10 m wind by applying a multiplier in the range of 1.3–1.5. Therefore, we decided to use a multiplier of 1.4 for convenience. This empirical relationship accounts, e.g., for plume rise and mixing into altitudes with larger wind speeds. For the present, we consider this approximation adequate for this first study, but we recognize that uncertainties (see next section) resulting from this estimate of the effective wind speed's normal may be reduced in the future by improved wind knowledge."

Reviewer 1: *P7-11, It would be most useful to have the wind direction adjustments clearly stated for every case either in the text or a table.*
Authors: We added this information for each scenario to the text of the corresponding sections. The adjustments were always between 17° (Baghdad) and 1° (Moscow).

Reviewer 1: *P8, L7: "larges" -> "largest"*
Authors: Done.

Reviewer 1: *P8, Sec 3.2: The enhancement near Lipetsk is huge and the fit is very good. Are there other sources in addition to the gas-fired power plant and the steel plant that could be relevant, for example, what about the city of Lipetsk (population 500,000)?*
Authors: Of course, there are also other CO_2 emitting industries in Lipetsk plus traffic etc. However, we do not have access to a emission data base on facility level for Lipetsk. In order to not give the impression that the steel plant and the power plant are the only two emitters, we have rephrased the first sentence of the chapter: "... shows the surrounding of Lipetsk (approx.

0.5 million inhabitants) with, among other industries, the Novolipetsk steel plant and the Lipetskaya TEC-2 gas-fired power plant ...". Additionally, we added the approximate population also to the Moscow, Baghdad, and Nanjing section.

Reviewer 1: *P9, Figure 1: I assume the hashed/shaded region is the Moscow urban area but I am not sure? Can the authors clarify in the figure caption?*
Authors: We added to the figure caption: "The hatched area corresponds to the urban area (World Urban Areas dataset, Geoportal of the University of California, *https://apps.gis.ucla.edu/geodata/dataset/world_ urban_ areas*)."

Reviewer 1: *P9, Sec 3.4: The OCO-2 flyby of the Matimba and Medupi power plants used in this work is over 80 km away. Nassar et al. (2017) also estimated the emissions from Matimba using OCO-2 data (but version 7) from a direct overpass in 2014 and a close flyby (7 km away) in 2016. Daily emission estimates from Nassar et al. converted to annual values are 12 MtCO2/a.*
Authors: Our flux estimate corresponds to the combined signal of the Matimba and Medupi power plant. Nevertheless, we added to our discussion: "Nassar et al. (2017) also estimated the emissions from the Matimba power plant (but not Medupi) using OCO-2 XCO_2 v7 data. For a direct overpass in 2014 and a close flyby ($\sim$7 km away) in 2016 they found fluxes, converted to annual values, of $12.1 \pm 3.9\,MtCO_2/a$ and $12.3 \pm 1.2\,MtCO_2/a$, respectively."

Reviewer 1: *P10, Sec 3.5. The Australian wildfires are clearly an example of an area source not a point source. The NO2 data show structure/heterogeneity in the area source. This makes it a poor candidate for the modeling approach applied that represents the plume with a Gaussian function. Furthermore, it makes little sense to report emissions in an annual unit in the case of a wildfire, which lasts on the order of days to weeks and would demonstrate temporal variability even over that limited time scale. For fossil fuel CO2 emissions from power plants or cities, there is also periodic (diurnal, weekly and seasonal variability) and non-periodic (plant shutdowns, heating/cooling linked to weather, etc.) variability, which also makes reporting emission rate estimates for shorter time scales more exact from a single overpass.*
Authors: We discuss that "the NO_2 (and less obvious maybe also the XCO_2) cross-section has two maxima" and that "the Gaussian fitting function cannot account for this". However, this is "not reflected in the overall good fit quality ($\chi^2 = 0.6$)" for the XCO_2 fit. This means, within the noise of the XCO_2 data, we cannot expect to significantly improve the XCO_2 fit by a more complex plume model. We rephrased the corresponding section which now reads: "The NO_2 (and less obvious also the XCO_2) cross-section has two maxima which cannot be accounted for by the Gaussian fitting function. However, this is not reflected in the good XCO_2 fit quality ($\chi^2 = 0.6$), but should be taken into account when valuing the results." The unit $MtCO_2/a$ is not unusual especially

for fluxes of power plants or other anthropogenic CO_2 emitters. Likewise driving a car at 50miles/hour does not mean that you actually drive the car one hour at that speed, our flux estimates are snapshots for the time of the overpass and are not necessarily representative for the annual average. This is particularly true for a wildfire but of course also for, e.g., a power plant if emissions vary in time. Within the section summary and conclusions we state that "our estimates are valid only for the time of the overpass...". Additionally, we emphasize this point within the sections for the Australian wildfires ("for the snapshot of the overpass, we computed a cross-sectional CO_2 flux ..."). The revised version makes this point also clear in a modified caption of Tab. 1: "Note that the cross-sectional flux results correspond to the instantaneous time of the overpass' whilst EDGAR and ODIAC emissions are annual or monthly averages..."

Reviewer 1: *P14, Figure 6. Nanjing seems to show two maxima in the NO2 image, which is also problematic to represent with a Gaussian function.*
Authors: As we do not fit the entire plume of CO_2 or NO_2 with a Gaussian plume model, additional upwind maxima in the NO_2 image pose no principle problem for the analysis of the plumes cross sectional flux. If an additional maximum is coming from an additional source, the source attribution becomes difficult. If it results from non steady state meteorological conditions (e.g., accumulated NO_2 during calm conditions), the plumes cross sectional flux may still be correctly derived but may become a poor estimate for the actual emission. For the Nanjing scene, EDGAR and ODIAC emissions suggest multiple significant emitters and we discuss in the section summary and conclusions: "... the scene includes a larger area of overlaying sources, making source attribution difficult."

Reviewer 1: *P14, L13: Why is 0.5/MtCO2/a the chosen minimum value?*
Authors: For most meteorological conditions, a source of 0.5 MtCO2/a per grid box is typically well below the detection limit of OCO-2. Additionally, given a limit of 0.5 MtCO2/a, the shown maps include a reasonable small amount of non-empty grid boxes so that the reader is easily able to find the largest emitters.

References

Brunner, D., Kuhlmann, G., Marshall, J., Clément, V., Fuhrer, O., Broquet, G., Löscher, A., and Meijer, Y.: Accounting for the vertical distribution of emissions in atmospheric CO_2 simulations, Atmospheric Chemistry and Physics, 19, 4541–4559, 2019.

Buchwitz, M., Schneising, O., Reuter, M., Heymann, J., Krautwurst, S., Bovensmann, H., Burrows, J. P., Boesch, H., Parker, R. J., Somkuti, P., Detmers, R. G., Hasekamp, O. P., Aben, I., Butz, A., Frankenberg, C., and Turner, A. J.: Satellite-derived methane hotspot emission estimates using a fast data-driven method, Atmospheric Chemistry and Physics, 17, 5751–5774, https://doi.org/10.5194/acp-17-5751-2017, URL https://www.atmos-chem-phys.net/17/5751/2017/, 2017.

Heymann, J., Reuter, M., Buchwitz, M., Schneising, O., Bovensmann, H., Burrows, J., Massart, S., Kaiser, J., and Crisp, D.: CO_2 emission of Indonesian fires in 2015 estimated from satellite-derived atmospheric CO_2 concentrations, Geophysical Research Letters, 44, 1537–1544, 2017.

Krings, T., Gerilowski, K., Buchwitz, M., Reuter, M., Tretner, A., Erzinger, J., Heinze, D., Pflüger, U., Burrows, J. P., and Bovensmann, H.: MAMAP - a new spectrometer system for column-averaged methane and carbon dioxide observations from aircraft: retrieval algorithm and first inversions for point source emission rates, Atmospheric Measurement Techniques, 4, 1735–1758, https://doi.org/10.5194/amt-4-1735-2011, URL https://www.atmos-meas-tech.net/4/1735/2011/, 2011.

Krings, T., Neininger, B., Gerilowski, K., Krautwurst, S., Buchwitz, M., Burrows, J. P., Lindemann, C., Ruhtz, T., Schüttemeyer, D., and Bovensmann, H.: Airborne remote sensing and in situ measurements of atmospheric CO_2 to quantify point source emissions, Atmospheric Measurement Techniques, 11, 721–739, https://doi.org/10.5194/amt-11-721-2018, URL https://www.atmos-meas-tech.net/11/721/2018/, 2018.

Nassar, R., Hill, T. G., McLinden, C. A., Wunch, D., Jones, D., and Crisp, D.: Quantifying CO_2 emissions from individual power plants from space, Geophysical Research Letters, 44, 2017.

Schneising, O., Heymann, J., Buchwitz, M., Reuter, M., Bovensmann, H., and Burrows, J. P.: Anthropogenic carbon dioxide source areas observed from space: assessment of regional enhancements and trends, Atmospheric Chemistry and Physics, 13, 2445–2454, https://doi.org/10.5194/acp-13-2445-2013, URL http://www.atmos-chem-phys.net/13/2445/2013/, 2013.

Varon, D. J., Jacob, D. J., McKeever, J., Jervis, D., Durak, B. O. A., Xia, Y., and Huang, Y.: Quantifying methane point sources from fine-scale satellite observations of atmospheric methane plumes, Atmospheric Measurement Techniques, 11, 5673–5686, https://doi.org/10.5194/amt-11-5673-2018, URL https://www.atmos-meas-tech.net/11/5673/2018/, 2018.

First of all, we thank reviewer 2 for his/her efforts in carefully reviewing our manuscript and his/her constructive comments.

Point-by-point answers to the comments of reviewer 2

General comments

Reviewer 2: *The number of cases studied is very small. Although 20 promising scenes were identified only six are shown in the manuscript. The authors should include the remaining cases, not as additional examples (except maybe in the supplement), but in order to have more cases to discuss and compare the results.*

Authors: Our intention by providing an approximate number of promising cases (20) was to give the reader an impression of how many cases can be expect when applying our current (pre-) selection method to a data set of several months. This does not mean, that we have thoroughly analyzed all of these 20 cases in detail which would make a significant amount of extra work. The focus of our study is on "demonstrating the benefits of simultaneous NO2 and XCO_2 measurements rather than on most accurate flux estimates" or on quantifying emissions of an as large as possible number of targets. Therefore, we do not see the immediate necessity to significantly lengthen the paper which also agrees with our interpretation of review 1 stating that "overall, this work is sufficient to demonstrate the value of coincident NO2 and CO2 satellite observations for estimating emissions".

Furthermore, we think that discussing these cases without showing them would be little helpful. As discussed, we use the NO_2 measurements "... to i) identify the source of the observed XCO_2 enhancements, ii) to exclude interference with potential additional remote upwind sources, iii) to manually adjust the wind direction, and iv) to put a constraint on the shape of the observed CO_2 plumes." All of these points, except the last, make use of the shown NO_2 maps. This means, when not showing the scenes, the reader would not be able to follow important parts of the analysis.

In case reviewer 2 is curious about !preliminary! results, we have added six more images at the end of this document.

Reviewer 2: *The manuscript lacks a detailed comparison of the examples and discussion of the result. A broad summary is given in the conclusions, but this should be moved to a designated section.*

Authors: Our manuscript is basically following the IMRaD (Introduction, Methods, Results, and Discussion, *https://en.wikipedia.org/wiki/IMRAD*, Hall, 2012) organizational structure which became the most prominent norm for the structuring of a scientific research article. We only slightly adapted the naming of the section headings of the first hierarchy level: *Methods* became *Data sets and methods* and *Discussion* became *Summary and conclusions.* Renaming the *Method* section is uncritical and many journals prefer heading style variants like *Methods and materials*, *Materials and methods*, or similar for the *Method* section. Usually, the *Discussion* section includes a summary and the conclusions. Both may or may not be part of the *Discussion* section or separate sections on the same hierarchy level as the *Discussion* section. Therefore, we agree, that the heading *Summary and conclusions* may be misleading and we renamed it to *Discussion and conclusions*. We wanted to keep "Conclusions" within the heading because the ACP template suggests to have a *Conclusions* top-level section.

We do not agree that this section does not include a thorough discussion of the results. Within this section, we compare our results with emission data bases and (in the revised version) also emission estimates of Nassar et al. (2017)): "For Moscow, we derived a cross-sectional flux of $76 \pm 33\,\mathrm{MtCO_2/a}$ which agrees (within its uncertainty) with ODIAC 2012 emissions of $102\,\mathrm{MtCO_2/a}$ ($88\,\mathrm{MtCO_2/a}$ for 08/2016) but not with EDGAR emissions of $195\,\mathrm{MtCO_2/a}$", "... this estimate agrees with EDGAR emissions of $23\,\mathrm{MtCO_2/a}$ but not with ODIAC emissions of $4\,\mathrm{MtCO_2/a}$", etc. We also discuss scenario specific potential reasons for differences: "... it is interesting to note that Georgoulias et al. (2019) found a strongly increasing trend ... for the tropospheric NO_2 concentrations in Baghdad ... hinting at strongly increasing CO_2 emissions in Baghdad ...", "... it shall be noted that GFED's emission estimate for the same time interval but one day before the OCO-2 overpass amounts to $252\,\mathrm{MtCO_2/a}$", low wind speed, acute angle of wind direction, etc. Additionally, we discuss the largest contributions to the total uncertainty, the potential effect of co-emitted aerosols, the differences between the emission data bases, the potential difference between cross sectional flux and source emission, etc. This means, whilst the *Results* section basically describes what is shown in the figures, several points within the *Summary and conclusions* section go far beyond a broad summary.

Reviewer 2: *Furthermore, the results of the flux estimates without including NO2 fields in the fit should be shown in the results and not only briefly mentioned in the conclusions (P15, L6ff).*

Authors: We modified the corresponding paragraph which now reads: "We repeated the flux estimation of all shown scenarios with such a setup and got fluxes of $61 \pm 27\,\mathrm{MtCO_2/a}$, $63 \pm 46\,\mathrm{MtCO_2/a}$, $75 \pm 29\,\mathrm{MtCO_2/a}$, $35 \pm 9\,\mathrm{MtCO_2/a}$, $166 \pm 44\,\mathrm{MtCO_2/a}$, and $119 \pm 28\,\mathrm{MtCO_2/a}$ for the Moscow, Lipetsk, Baghdad, Medupi/Matimba, Australian wildfires, and Nanjing scenario, respectively. The derived fluxes are consistent within their uncertainty with our main results shown in Tab. 1, but the uncertainty contribution due to the noise in the XCO_2 data increased by 34% from $4.7\,\mathrm{MtCO_2/a}$ to $6.3\,\mathrm{MtCO_2/a}$ on average."

Reviewer 2: *The connection between this study and the proposed CO2M mission, which is emphasized in the abstract and the conclusions, is not well presented. The authors used the NO2 fields to identify the location of the source outside the OCO-2 swath and to screen for potential sources upstream. Both will not be possible with the CO2M mission, if CO2 and NO2 instrument*

would have the same swath as currently proposed. In addition, it might also not be necessary for CO2M to use NO2 to identify the source outside the swath, because CO2M's swath will be significantly wider than OCO-2's swath. A major advantage of the NO2 observations is likely the potential for improving the fit of the Gaussian (see previous comment), which should be presented more prominently.
Authors: As summarized in the abstract (and the last section), we use the NO_2 measurements not only for these two purposes but also to adjust the wind direction and to constrain the shape of the CO_2 plumes. CO2M will have a much wider swath compared to OCO-2, so that there is a good chance to see large parts of the plume including the location of the source plus potential upwind sources within the swath even if the NO_2 instrument would only cover the same swath as the CO_2 instrument. Additionally, it has not yet been finally decided how large the swath width of the NO_2 instrument will be, i.e., there is a chance that it might become wider than the CO_2 instrument. As discussed within the conclusions, "the noise of the XCO_2 retrievals contributes only with $1\,MtCO_2/a$ to $8\,MtCO_2/a$ to the total error". This error enhances by about 34% when ignoring the NO_2 measurements. In other words, for the method as presented, other error components are clearly dominating which is why we put the fit improvement not more into focus. However, this will change for CO2M, because "the meteorology related uncertainties will reduce (Varon et al., 2018) because deviations from steady state conditions can average out and are, therefore, less critical if the entire plume structure is sampled rather than only a cross-section". In this case, the uncertainties introduced by the XCO_2 retrievals will become more important and the "imaging capabilities (of CO2M) will reduce the uncertainty of the inferred emissions due to measurement noise simply because of the increased number of soundings. Additionally, simultaneous XCO_2 and NO_2 observations from the same platform will allow stricter constraints on the plume shape."

Specific comments

Reviewer 2: *P2, L5ff: Consider re-formulating, e.g.: "... to halve [...] emissions each decade after reaching peak emissions in 2020"*
Authors: The sentence now reads: "Actions need to be taken to halve anthropogenic greenhouse gas emissions (including CO_2) each decade after reaching peak emissions in 2020 (Rockström et al., 2017)."

Reviewer 2: *P2, L21-23: Consider to remove, because the detailed chemistry seems not relevant for the study.*
Authors: We would prefer to keep the paragraph as is, because the complex chemical relations are the reason for potential differences in the plume shape of CO_2 and NO_2.

Reviewer 2: *P2, L27: Add the resolution of the NO2 instrument.*
Authors: The most important specifications (for our study) of the NO_2 instrument are listed in Sec. 2.2 ("... spatial resolution of 3.5 km×7 km at nadir ...").

Reviewer 2: *P2, L29: Clarify the term "localized small scale".*
Authors: The sentence now reads: "... which can be attributed to localized (up to city-scale) emissions ..."

Reviewer 2: *P3, L10f: Consider changing "The data set ..." to "The product ..." to make it clear that the filtering is part of the OCO-2 L2 Lite product.*
Authors: Done.

Reviewer 2: *P4, L1: Please explain the term "viewing angle corrected". Are these geometric air mass factors?*
Authors: In this context, we are interested in the scatter of the slant (not vertical) columns, which is why we corrected only for the viewing angle but not the solar zenith angle, i.e., NO_2 slant columns have been corrected for the viewing angle dependent change in the geometric air mass factor. Correcting for changes in the viewing angle is necessary because, otherwise, the inferred scatter would comprise not only changes due to instrumental noise but also the variability of the viewing angle.

Reviewer 2: *P4, L4-9: The paragraph might be easier readable, if it first explains the approach used in this study and briefly contrasts it the "normal" approach.*
Authors: We have the impression that describing first what we have done, renders the description of the "normal" approach a bit superfluous. However, we added "usually" to the first sentence, suggesting that an alternative method will be presented in the following: "In order to extract the tropospheric vertical columns, usually, first the stratospheric contribution ..."

Reviewer 2: *P4, L13: It would be useful to have the time difference between OCO-2 and Tropomi for the six examples presented in the manuscript.*
Authors: The actual time differences per scenario are shown in the figures and the figure captions read: "... and time difference between OCO-2 and S5P overpass are also listed."

Reviewer 2: *P4, L22: Please specify if three times lower resolution is temporal, spatial or both and, if spatial resolution, if it is grid cell area or length. Maybe it's better to just write the resolution of the product.*
Authors: The sentence now reads: "This data archive provides also an uncertainty estimate of the wind information from an ensemble statistic but at a reduced resolution of $0.5^{\circ}\times0.5^{\circ}\times$three hours."

Reviewer 2: *P5, L7-8: This is not a constraint on the width of the CO2 Gaussian function, if CO2 and NO2 values are fitted simultaneously, but using the same width for fitting both CO2 and NO2 Gaussian function. It would be a constraint if the NO2 plume is fitted first and afterwards the CO2 plume is fitted using the coefficient obtained from the NO2 fit.*
Authors: We now decribe more precisely how we constrain the FWHM fit by NO_2 only: "We force the FWHM to be constrained entirely by the NO_2 measurements by setting the CO_2 part of the corresponding Jacobian artificially to zero. However, we expect only little differences to a combined FWHM fit because of the lower relative noise of the NO_2 measurements."

Reviewer 2: *P5, L13: Please clarify if a Level-2 or Level-3 product is used for the fit.*
Authors: We use the co-located XCO_2 and NO_2 values as described in Sec. 2.3 for the fit. This means the XCO_2 values are those given in the OCO-2 L2 product and the NO_2 values correspond to averages within the CO_2 footprints. Because of OCO-2's much finer spatial resolution, most of the NO_2 averages are being build from a single S5P sounding only. The sentence now reads: "Specifically, the co-located NO_2 and XCO_2 values ..."

Reviewer 2: *P5, L22: The equation would be more readable without the unit conversions. The equation could be split in two.*
Authors: We removed the unit conversions from Eq. 2 and rephrased the paragraph which now reads:

Integration over the Gaussian enhancement results in the cross-sectional CO_2 flux F_{CO_2} (mass of CO_2 per time) of the plume depending on the FWHM a_4, the amplitude of the XCO_2 enhancement a_7, the effective wind speed v_e within the plume normal to the OCO-2 orbit, and the number of dry air particles in the atmospheric column n_e:

$$F_{CO_2} = \frac{1}{2} \sqrt{\frac{\pi}{ln(2)}} \frac{M_{CO_2}}{N_A} \; n_e \; a_4 \; a_7 \; v_e$$

Here, M_{CO_2} is the molar mass of CO_2 (44.01 g/mol) and N_A the Avogadro constant ($6.02214076 \cdot 10^{13}\,\mathrm{mol}^{-1}$).

...

For a hydrostatic atmosphere with a standard surface pressure of 1013hPa, n_e is about $2.16 \cdot 10^{25}\,\mathrm{cm}^{-2}$ and the cross-sectional CO_2 flux F_{CO_2} (Eq. 2) in units of $MtCO_2/a$ becomes approximately

$$F_{CO_2} \approx 0.53 \; \frac{\mathrm{MtCO_2}}{\mathrm{a}} \; \frac{a_4}{\mathrm{km}} \; \frac{a_7}{\mathrm{ppm}} \; \frac{v_e}{\mathrm{m/s}}$$

given that the FWHM a_4, the amplitude of the XCO_2 enhancement a_7, and the effective wind speed v_e are provided in the units km, ppm, and m/s, respectively. As n_e approximately scales with the surface pressure, Eq. 3 may be easily adapted to other meteorological conditions.

Reviewer 2: *P5, L27: Does the OCO-2 product have not air columns that could be used instead?*
Authors: We are using the bias corrected "lite" product which does not include dry air columns but we have to read the ECMWF data in order to obtain the wind information anyhow.

Reviewer 2: *P6, L3: Please add how sensitive the factor (i.e. 0.53) is to surface pressure, to provide a range in which this approximation might be used.*
Authors: We added: "As n_e approximately scales with the surface pressure, Eq. 3 may be easily adapted to other meteorological conditions."

Reviewer 2: *P6, L24: Please state typical values for the uncertainty of the wind speed in the ERA5 data.*
Authors: The sentence now reads: "The uncertainties of the wind components are read from the ECMWF ERA5 data archive resulting in total wind speed uncertainties ranging from 0.18 m/s to 0.33 m/s for the analyzed scenarios."

Reviewer 2: *P7, L5: Are the 100 co-locations for Level-2 or Level-3?*
Authors: The XCO_2 values are as in the OCO-2 L2 product and the NO_2 values correspond to averages within the CO_2 footprints (see also discussion above and Sec. 2.3).

Reviewer 2: *P15, L1ff: The major advantage of the NO2 instrument here would be the wider swath and thus having CO2 instrument with a wider swath should bring the same advantage without the need for an additional NO2 instrument. The authors should consider discussing if (or why not) having a CO2 instrument with a wide swath is (not) an option.*
Authors: As visible in the figures and briefly mentioned in Sec. 3.1 ("... larger relative noise of the XCO2 retrievals ..."), the noise of the NO_2 retrievals is about 5 times lower than for XCO_2 relative to the expected enhancements. This will drastically improve the plume detection and also allow to better constrain the plume shape. Additionally, the background variability due to natural sources/sinks is much larger for XCO_2 than for NO_2. We modified parts of the abstract, introduction, and summary and conclusions in order to emphasize the difference in the noise performances.

Within the abstract and similarly within the introduction, one now can read: "However, regional column-average enhancements of individual point sources are usually small compared to the background concentration and its natural variability and often not much larger than the satellite's measurement noise. ... It has a short lifetime of the order of hours so that NO_2 columns often greatly exceed background and noise levels of modern satellite sensors near sources which makes it a suitable tracer of recently emitted CO_2."

Within the discussion we added: "Despite less strict quality filtering is needed, peak enhancements of NO_2 columns near sources can be retrieved from satellites with much lower relative noise than this is the case for XCO_2."

Reviewer 2: *P15, L22: Please explain the term "steady state conditions" in the paper.*
Authors: The first occurrence of this term is at P6 L12 and we modified it to "... under steady state (temporally invariant) conditions ...".

Reviewer 2: *Figure 1-6: The corrected wind arrow looks very subjectively. It might help to draw the arrow centered on the XCO2 swath where the arrow should be a perpendicular to the plume.*
Authors: We do not quite understand the suggestion of the reviewer because non of the arrows should be perpendicular to the plume. For the analyzes of the Gaussian enhancement, we are not considering the across track dimension of the OCO-2 swath. This means, all values are referenced by its distance in flight direction (or time) as plotted in Fig. 1-6c. In the along track dimension, the origin of the arrows is determined by the position of the maximum of the Gaussian XCO_2 fit. In the across track dimension a more or less arbitrary sounding is selected.

Reviewer 2: *Table 1: Mention that the single sounding uncertainty (0.4-0.7 ppm) provided the OCO-2 product was used for computing the flux uncertainty, because evaluation with TCCON found a significant larger value (1.3 ppm).*
Authors: The table caption now reads: "... the XCO_2 precision as reported in the data product, and the NO_2 precision as reported in the data product."

Reviewer 2: *Table 1: Add to the columns that estimated cross sections are instantaneous; EDGAR and ODIAC are annual or monthly emissions.*
Authors: We added to the table caption: "Note that the cross-sectional flux results correspond to the instantaneous time of the overpass' whilst EDGAR and ODIAC emissions are annual or monthly averages; GFED emissions correspond to six hourly averages (see Sec. 2.4)."

Technical corrections

Reviewer 2: *P1, L10: XCO2 was already defined in line 3*
Authors: We removed the second occurrence.

Reviewer 2: *P5, L5: Consider changing "... first degree polynomial (i.e. a linear polynomial) ..." to "... a linear polynomial ...".*

Authors: Done.

Reviewer 2: *P5, L6: Consider adding commas before "accounting" and after "values".*
Authors: Done.

References

Georgoulias, A. K., van der A, R. J., Stammes, P., Boersma, K. F., and Eskes, H. J.: Trends and trend reversal detection in 2 decades of tropospheric NO_2 satellite observations, Atmospheric Chemistry and Physics, 19, 6269–6294, https://doi.org/10.5194/acp-19-6269-2019, URL `https://www.atmos-chem-phys.net/19/6269/2019/`, 2019.

Hall, G. M.: How to write a paper (5th ed.), Wiley-Blackwell, BMJ Books, ISBN: 978-0-470-67220-4, 2012.

Nassar, R., Hill, T. G., McLinden, C. A., Wunch, D., Jones, D., and Crisp, D.: Quantifying CO_2 emissions from individual power plants from space, Geophysical Research Letters, 44, 2017.

Rockström, J., Gaffney, O., Rogelj, J., Meinshausen, M., Nakicenovic, N., and Schellnhuber, H. J.: A roadmap for rapid decarbonization, Science, 355, 1269–1271, 2017.

Varon, D. J., Jacob, D. J., McKeever, J., Jervis, D., Durak, B. O. A., Xia, Y., and Huang, Y.: Quantifying methane point sources from fine-scale satellite observations of atmospheric methane plumes, Atmospheric Measurement Techniques, 11, 5673–5686, https://doi.org/10.5194/amt-11-5673-2018, URL `https://www.atmos-meas-tech.net/11/5673/2018/`, 2018.

Figures (!preliminary!)

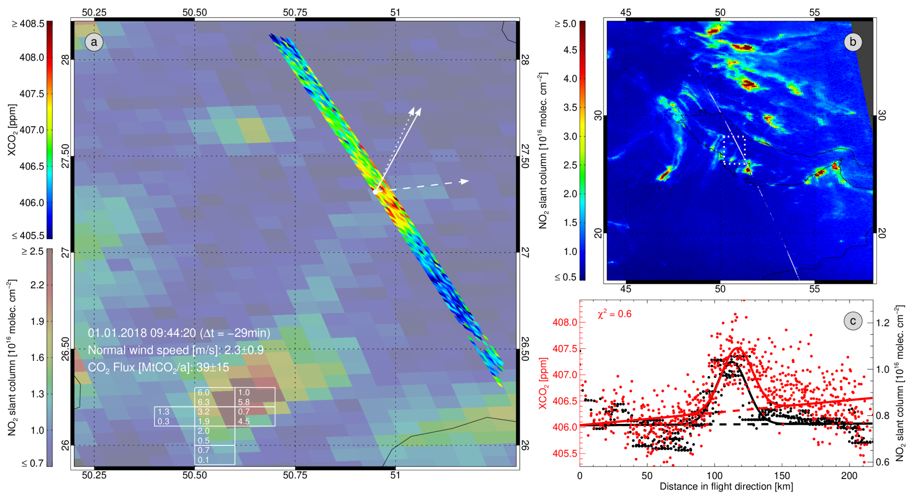

Figure 1: As paper Fig. 1 but for Bahrain on January 1, 2018.

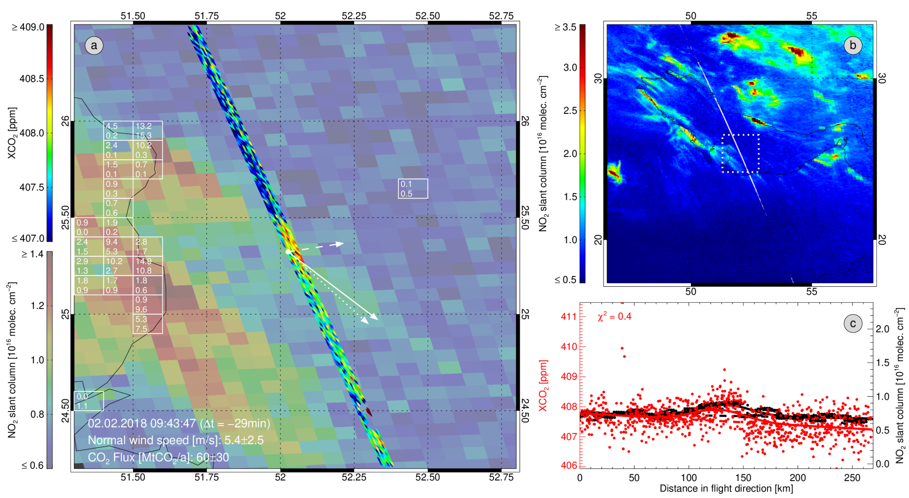

Figure 2: As paper Fig. 1 but for Qatar on February 2, 2018.

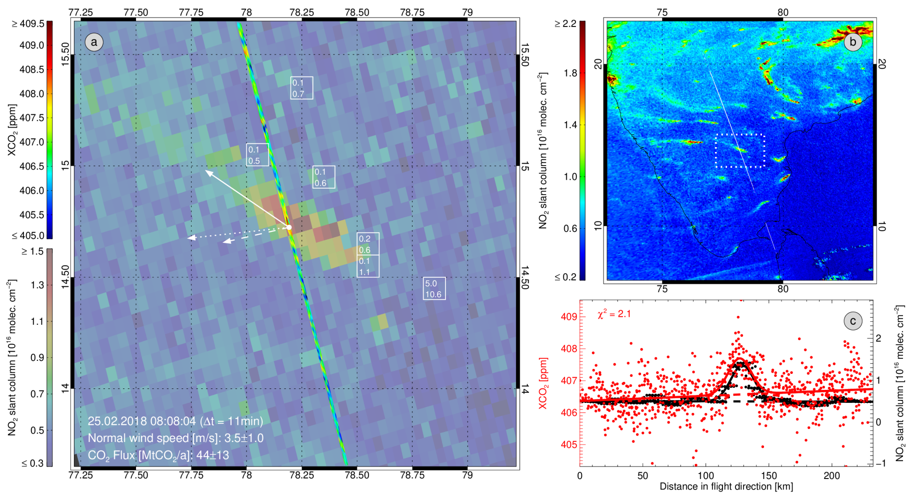

Figure 3: As paper Fig. 1 but for India on February 25, 2018.

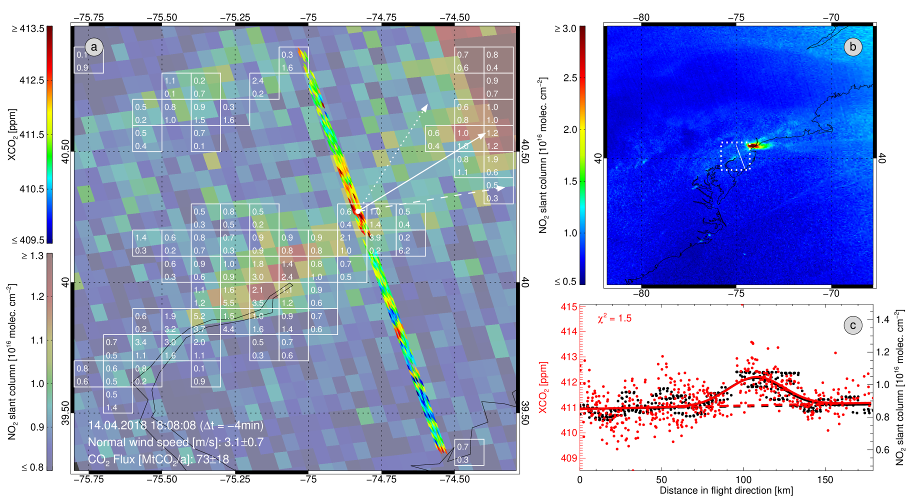

Figure 4: As paper Fig. 1 but for the USA on April 14, 2018.

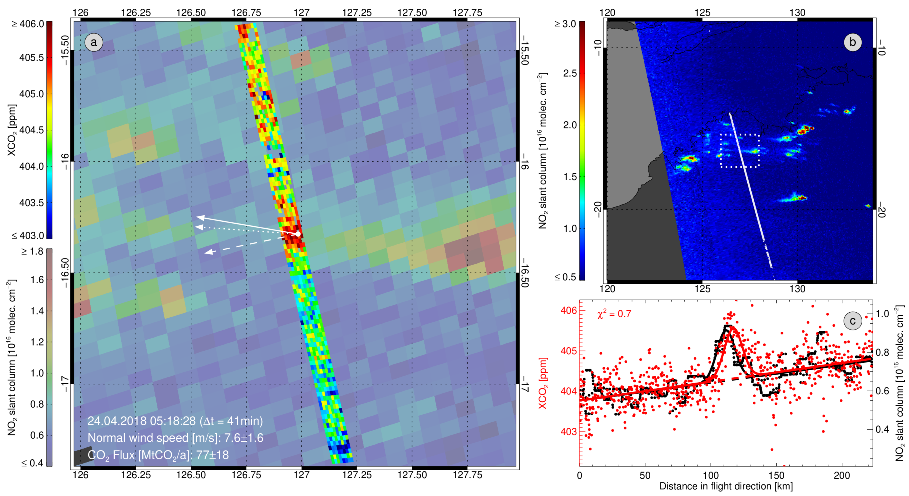

Figure 5: As paper Fig. 1 but for Australia on April 24, 2018.

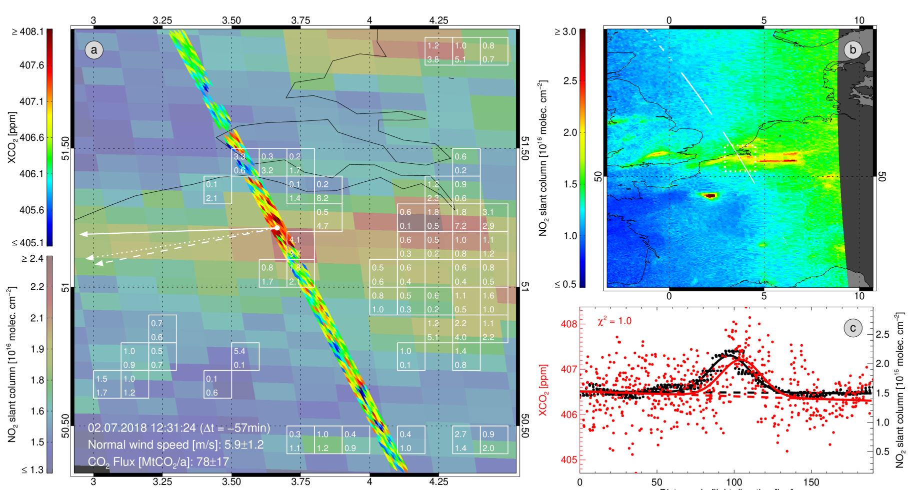

Figure 6: As paper Fig. 1 but for Belgium on July 2, 2018.

Towards monitoring localized CO_2 emissions from space: co-located regional CO_2 and NO_2 enhancements observed by the OCO-2 and S5P satellites

Maximilian Reuter[1], Michael Buchwitz[1], Oliver Schneising[1], Sven Krautwurst[1], Christopher W. O'Dell[2], Andreas Richter[1], Heinrich Bovensmann[1], and John P. Burrows[1]

[1]Institute of Environmental Physics, University of Bremen, Germany
[2]Colorado State University, Fort Collins, CO, USA

Correspondence: Maximilian Reuter (mail@maxreuter.org)

Abstract. Despite its key role for climate change, large uncertainties persist in our knowledge of the anthropogenic emissions of carbon dioxide (CO_2) and no global observing system exists allowing to monitor emissions from localized CO_2 sources with sufficient accuracy. The Orbiting Carbon Observatory-2 (OCO-2) satellite ~~can retrieve~~ allows retrievals of the column-average dry-air mole fractions of CO_2 (XCO_2). However, regional column-average enhancements of individual point sources are usually small compared to the background concentration and its natural variability and often not much larger than the satellite's measurement noise. This makes the unambiguous identification and quantification of anthropogenic emission plume signals challenging. NO_2 is co-emitted with CO_2 when fossil fuels are combusted at high temperatures. It has a short lifetime of the order of hours so that NO_2 columns often ~~exceed background levels by orders of magnitude near sources making~~ greatly exceed background and noise levels of modern satellite sensors near sources which makes it a suitable tracer of recently emitted CO_2. Based on six case studies (Moscow, Russia; Lipetsk, Russia; Baghdad, Iraq; Medupi and Matimba power plants, South Africa; Australian wildfires; and Nanjing, China), we demonstrate the usefulness of simultaneous satellite observations of NO_2 and ~~the column-average dry-air mole fraction of CO_2 (~~XCO_2~~)~~. For this purpose, we analyze co-located regional enhancements of XCO_2 observed by OCO-2 and NO_2 ~~observed by~~ from the Sentinel-5 Precursor (S5P) satellite and estimate the CO_2 plume's cross-sectional fluxes. We take advantage of the nearly simultaneous NO_2 measurements with S5P's wide swath and small measurement noise by identifying the source of the observed XCO_2 enhancements, excluding interference with remote upwind sources, allowing to adjust the wind direction, and by constraining the shape of the CO_2 plumes. We compare the inferred cross-sectional fluxes with the Emissions Database for Global Atmospheric Research (EDGAR), the Open-Data Inventory for Anthropogenic Carbon dioxide (ODIAC), and, in the case of the Australian wildfires, with the Global Fire Emissions Database (GFED). The inferred cross-sectional fluxes range from ~~32~~31 $MtCO_2$/a to ~~158~~153 $MtCO_2$/a with uncertainties (1σ) between 23% and 72%. For the majority of analyzed emission sources, the estimated cross-sectional fluxes agree within their uncertainty with either EDGAR or ODIAC or lie in between them. We assess the contribution of multiple sources of uncertainty and find that the dominating contributions are related to the computation of the effective wind speed normal to the plume's cross-section. The planned European Copernicus anthropogenic CO_2 monitoring mission (CO2M) will not only provide precise measurements with high spatial resolution but also imaging capabilities with a wider swath of simultaneous XCO_2 and NO_2

observations. Such a mission, in particular as a constellation of satellites, will deliver CO_2 emission estimates from localized sources at an unprecedented frequency and level of accuracy.

1 Introduction

Carbon dioxide (CO_2) is the most important anthropogenic greenhouse gas and driver for climate change. By September 2018, 195 member states of the UNFCCC (United Nations Framework Convention on Climate Change) have signed the Paris agreement with the long-term goal to keep the increase in global average temperatures relative to pre-industrial levels well below 2°C. Actions need to be taken to halve anthropogenic greenhouse gas emissions (including CO_2) each decade after reaching a maximum peak emissions in 2020 (Rockström et al., 2017). However, there are still large uncertainties in the anthropogenic emissions and no global observing system exists allowing to monitor country emissions and their changes with sufficient accuracy (e.g., Ciais et al., 2014; Pinty et al., 2017).

CO_2 is long-lived and well-mixed in the atmosphere and its largest gross fluxes are of natural origin (photosynthesis and respiration). As a result, regional (column-average) enhancements of individual anthropogenic point sources are usually small compared with the background concentration and its natural variability and often not much larger than the satellite's measurement noise (Bovensmann et al., 2010). This makes the identification of anthropogenic plume signals with past (SCIAMACHY (SCanning Imaging Absorption SpectroMeter for Atmospheric CHartographY, Burrows et al., 1995; Bovensmann et al., 1999)) and current (GOSAT (Greenhouse Gases Observing Satellite, Kuze et al., 2009), OCO-2 (Orbiting Carbon Observatory-2, Crisp et al., 2004)) satellite sensors difficult and the quantification of anthropogenic emissions a challenging task. Usually, it the latter requires knowledge of the source position and assumptions on plume formation (e.g., Nassar et al., 2017; Heymann (e.g., Nassar et al., 2017; Heymann et al., 2017) or statistical approaches applied on larger areas (e.g., Kort et al., 2012; Schneising et al., 20 and/or time periods (e.g., Schneising et al., 2013; Buchwitz et al., 2017).

Reuter et al. (2014) followed an alternative approach to identify anthropogenic regional CO_2 enhancements by analyzing simultaneous satellite observations of tropospheric nitrogen dioxide (NO_2) vertical columns and column-average dry-air mole fractions of CO_2 (XCO_2). Nitrogen monoxide (NO) is formed and emitted to the atmosphere when fossil fuels are combusted at high temperatures. In the atmosphere, it reacts rapidly with ozone (O_3) and at a much slower rate via a termolecular reaction with oxygen (O_2) to form NO_2. The tropospheric daytime concentrations of NO_2 are coupled with the concentrations of NO and O_3 by the Leighton photo-stationary state. NO_2 has a short lifetime of the order of hours so that its vertical column densities often exceed background levels by orders of magnitude greatly exceed background and noise levels of modern satellite sensors near sources (Richter et al., 2005) making it a suitable tracer of recently emitted CO_2.

In contrast to SCIAMACHY used by Reuter et al. (2014), OCO-2 has no NO_2 sensor aboard. However, with the launch of the S5P satellite (Sentinel-5 Precursor, Veefkind et al., 2012) in October 2017, NO_2 observations with unprecedented spatial resolution and global daily coverage became available. Here we use this data to identify OCO-2 XCO_2 enhancements which can be attributed to localized small scale (up to city-scale) emissions for which we estimate the plume's cross-sectional CO_2 fluxes.

In the next section, we describe the used OCO-2 XCO_2 and S5P NO_2 data sets and the developed co-location method. In section 2, we describe the used plume detection and scenario selection method as well as the cross-sectional flux estimation method. The results of our case study analyses are presented and discussed in section 3 and 4, respectively.

2 Data sets and methods

2.1 XCO_2

The Orbiting Carbon Observatory-2 (OCO-2, Crisp et al., 2004) was launched in 2014 aiming at continuing and improving XCO_2 observations from space. OCO-2 is part of the A-train satellite constellation and flies in a sun-synchronous orbit whose ascending node crosses the equator on 13:36 local time. It measures the solar backscattered radiance in three independent wavelength bands in the spectral regions of the near infrared (NIR) and short wave infrared (SWIR): the O_2-A band at around 760 nm, the weak CO_2 band at around 1610 nm, and the strong CO_2 band at around 2060 nm. OCO-2 is operated in a near-push-broom fashion and has eight parallelogram-shaped footprints across track with a spatial resolution at ground of $\lesssim$1.29 km×2.25 km.

We use NASA's operational bias corrected OCO-2 L2 Lite XCO_2 product v9 (Kiel et al., 2019, see Fig. 1a for an example) which we obtained from *https://daac.gsfc.nasa.gov*. The ~~data set~~ product is rigorously pre- and post-filtered for potentially unreliable soundings including, e.g., cloud and aerosol contaminated scenes. Additionally, the OCO-2 retrieval algorithm accounts for light scattering at optically thin aerosol layers by fitting the optical depth and height of two lower-atmosphere aerosol layers and the optical depth of a stratospheric aerosol layer (O'Dell et al., 2018). The OCO-2 v9 data set has an improved bias correction approach that results in reduced biases particularly over areas of rough topography.

The OCO-2 XCO_2 product includes an uncertainty estimate which we use for our study. For the selected scenarios, the reported single sounding uncertainty lies typically in the range of 0.4 ppm to 0.7 ppm which is similar to estimates based on the standard deviation of the difference of succeeding soundings. The validation study of Reuter et al. (2017) estimated that the single sounding precision relative to ground based Total Carbon Column Observing Network (TCCON) data is about 1.3 ppm. However, this includes, e.g., the noise of the validation data set and a larger pseudo-noise component due to spatial and temporal representation errors when co-locating OCO-2 with the validation data and it shall be noted that the study of Reuter et al. (2017) analyzed a predecessor NASA OCO-2 XCO_2 data set (v7 instead of v9).

2.2 NO_2

The TROPOspheric Monitoring Instrument (TROPOMI) on Sentinel-5 Precursor was launched in October 2017 into a sun-synchronous orbit with an ascending node local equator crossing time of 13:30 (Veefkind et al., 2012). TROPOMI is a nadir viewing imaging grating spectrometer for the UV/visible spectral region with additional channels in the NIR and SWIR, extending the existing data records of the GOME (Global Ozone Monitoring Experiment), SCIAMACHY, OMI (Ozone Monitoring Instrument), and the GOME-2 missions. It has a swath width of about 2600 km and in comparison to previous instruments a much better spatial resolution of 3.5 km×7 km at nadir at similar signal to noise ratio per measurement. Here we use radiances in the spectral region 425 nm–465 nm to retrieve NO_2 slant columns with a standard Differential Optical Absorption Spectroscopy (DOAS) retrieval developed for previous satellite instruments (Richter et al., 2011), followed by a de-striping step as described by Boersma et al. (2007). Slant columns are defined as the absorber concentration integrated along the light path, and thus depend on both, the atmospheric NO_2 profile, and the light path of the individual measurement.

Evaluation of the scatter of viewing angle corrected NO_2 slant columns over a clean Pacific region (10°S–10°N, 160°E–230°E) indicates that the random noise (1σ) of our S5P slant columns is typically $5 \cdot 10^{14}$ molec./cm^2 . (enhancements near sources often exceed 10^{16} molec./cm^2). For individual soundings, the uncertainty can differ depending on viewing geometry and surface reflectance.

In order to extract the tropospheric vertical columns, usually, first the stratospheric contribution to the retrieved slant columns needs to be removed and then the light path dependency of the remaining tropospheric slant columns is corrected for by dividing through a scene dependent air mass factor. In this study, another approach is taken as only localized enhancements are evaluated. By subtracting the surrounding background values (section 2.5), both the stratospheric contribution and any tropospheric background are removed from the signal as they are both smooth on scales of a few tens of kilometers discussed here. What remains is the slant column plume signal of the lower troposphere from which we derive information on the CO_2 plume.

2.3 Co-location of OCO-2 and S5P data

OCO-2 and S5P fly both in sun-synchronous orbits with similar equator crossing times of their ascending nodes and orbit times of about 100 minutes. S5P has a swath width of about 2600 km which provides nearly global coverage each day. For these reasons, basically each scene observed by OCO-2 is also observed by S5P within a maximum time difference of about 50 minutes. We project the S5P and OCO-2 data of the same day in a surrounding of a potential target on a high resolution (0.001° × 0.001°) grid to compute NO_2 averages representative for the footprints of the CO_2 soundings (see Fig. 1c for an example).

2.4 Geophysical data bases

As input for the computation of the cross-sectional fluxes (section 2.5), we compute the number of dry air particles in the atmospheric column from meteorological profiles which we read at the same time with the wind information from the ECMWF (European Centre for Medium range Weather Forecast) ERA5 (fifth generation of ECMWF atmospheric reanalyzes) data archive at 0.25°×0.25°×hourly resolution. This data archive provides also an uncertainty estimate of the wind information (at three times lower resolution) from an ensemble statistic but at a reduced resolution of about 0.5°×0.5°×three hours.

We compare the inferred cross-sectional CO_2 fluxes with the following emission data bases. The Emissions Database for Global Atmospheric Research (EDGAR v4.3.2, *https://edgar.jrc.ec.europa.eu*) provides information on anthropogenic CO_2 emissions at 0.1°×0.1°×annually resolution. EDGAR v4.3.2 ends in 2012 and we use the data of that year for our comparisons. The Open-Data Inventory for Anthropogenic Carbon dioxide (ODIAC v2017, *http://db.cger.nies.go.jp/dataset/ODIAC*, Oda et al., 2018) provides also information on annual anthropogenic CO_2 emissions but at a higher finer resolution (1 km×1 km×monthly) and the data base ends in 2016. For the reason of comparability, we re-gridded the ODIAC emissions to the EDGAR resolution (0.1°×0.1°×annual) and use 2012 data as baseline. Additionally, we use ODIAC v2017 data re-gridded to 0.1°×0.1°×monthly resolution. The Global Fire Emissions Database (GFED v4.1s, *https://www.globalfiredata.org*) provides information on CO_2 emissions from wildfires at a resolution of 0.25°×0.25°×3- hours which we re-gridded to 0.1°×0.1° resolution for a six hours average ending approximately at the time of the overpass.

2.5 Flux estimation

S5P's spatial resolution is considerably coarser than that of OCO-2. Consequently for our case studies, we concentrate on plumes which are significantly larger than the swath width of OCO-2. This means that for the selected scenesscenarios, OCO-2 sees actually only a cross-section of a plume (see Fig. 1c for an example).

We model the cross-sectional NO_2 columns along the OCO-2 orbit by a first degree polynomial (i.e., a linear polynomial) linear polynomial, accounting for large scale variations of the background values, overlayed by a Gaussian function describing the enhancement within the plume. Simultaneously, the cross-sectional CO_2 concentrations are modeled in a similar manner. However, the width of the CO_2 Gaussian function is constrained to equal the width of the NO_2 Gaussian function. This means, the plume shape is determined from the NO_2 measurements, but we allow for a shifted position of the maximum in order to account for potential plume displacements resulting from different overpass times. Additionally, it shall be noted that the CO_2 and NO_2 plumes may have small differences, e.g., due to different decay rates of NO_2 in different altitudes. These differences, however, are considered minor compared with the precision of the XCO_2 soundings. Specifically, the co-located NO_2 and XCO_2 values along the distance in OCO-2's flight direction x are fitted with the maximum likelihood method by the following vector function:

$$\begin{pmatrix} NO_2 \\ XCO_2 \end{pmatrix} = \begin{pmatrix} a_0 + a_1\, x + a_2\, e^{-4\, ln(2)\, (x-a_3)^2\, a_4^{-2}} \\ a_5 + a_6\, x + a_7\, e^{-4\, ln(2)\, (x-a_8)^2\, a_4^{-2}} \end{pmatrix} \qquad (1)$$

The free fit parameters a_{0-8} correspond to the polynomial coefficients of the background values ($a_{0,1,5,6}$), the amplitudes ($a_{2,7}$), shifts ($a_{3,8}$), and the full width at half maximum (FWHM, a_4) of the Gaussian functions. We force the FWHM to be constrained entirely by the NO_2 measurements by setting the CO_2 part of the corresponding Jacobian artificially to zero. However, we expect only little differences to a combined FWHM fit because of the lower relative noise of the NO_2 measurements.

Integration over the Gaussian enhancement results in the cross-sectional CO_2 flux F_{CO_2} (in units of MtCOmass of CO_2 /aper time) of the plume depending on the FWHM a_4(in km), the amplitude of the XCO_2 enhancement a_7(in ppm), the effective wind speed v_e (in m/s) within the plume normal to the OCO-2 orbit, and the number of dry air particles in the atmospheric column n_e (in cm^{-2}):

$$F_{\mathrm{CO_2}} = \frac{1}{2}\sqrt{\frac{\pi}{ln(2)}} \cdot 3600 \cdot 24 \cdot 365 \, \frac{\mathrm{s}}{\mathrm{a}} \, \frac{M_{\mathrm{CO_2}}}{N_A} \, \frac{M_{\mathrm{CO_2}} \cdot \frac{10^{-12}\mathrm{Mt}}{\mathrm{g}}}{N_A} \cdot n_e \, \frac{10^4 \mathrm{cm}^2}{\mathrm{m}^2} \cdot a_4 \, \frac{10^3 \mathrm{m}}{\mathrm{km}} \cdot a_7 \, \frac{10^{-6}}{\mathrm{ppm}} \cdot v_e \qquad (2)$$

Here, $M_{\mathrm{CO_2}}$ is the molar mass of CO_2 (in 44.01 g/mol) and N_A the Avogadro constant ($6.02214076 \cdot 10^{13}$ mol^{-1}). We approximate the number of dry air particles n_e and the effective wind speed's normal v_e from ECMWF ERA5 meteorological profiles at the position of the maximum of the fitted Gaussian XCO_2 function. In regions with large variations of the surface elevation or wind conditions within the plume's cross-section, it might be appropriate to account for variations in the number of dry air particles and/or the wind conditions when integrating over the Gaussian enhancement.

We manually adjust the ECMWF wind direction (not the wind speed) to subjectively fit the plume direction observed in the NO_2 fields (e.g., Fig. 1a). The manual adjustment to wind direction but not wind speed is similar to the approaches of, e.g., Krings et al. (2011) or Nassar et al. (2017).

For a hydrostatic atmosphere with a standard surface pressure of 1013hPa, n_e is about $2.16 \cdot 10^{25}$ cm^{-2} and the cross-sectional CO_2 flux $F_{\mathrm{CO_2}}$ (Eq. 2becomes approximately:) in units of MtCO_2/a becomes approximately

$$F_{\mathrm{CO_2}} \approx 0.53 \, \frac{\mathrm{MtCO_2}}{\mathrm{a}} \, a_4 \frac{a_4}{\mathrm{km}} \, a_7 \frac{a_7}{\mathrm{ppm}} \, v_e \frac{v_e}{\mathrm{m/s}} \qquad (3)$$

given that the FWHM a_4, the amplitude of the XCO_2 enhancement a_7, and the effective wind speed v_e are provided in the units km, ppm, and m/s, respectively. As n_e approximately scales with the surface pressure, Eq. 3 may be easily adapted to other meteorological conditions.

As discussed by Brunner et al. (2019), the plume height (and subsequently the wind speed in plume height) depends on many aspects like emission height, stack geometry, flue gas exit velocity and temperature, meteorological conditions, etc. Some of these parameters are not known for many sources and their explicit consideration would go beyond the scope of this study focusing on demonstrating the benefits of simultaneous NO_2 and XCO_2 measurements rather than on most accurate flux estimates. Varon et al. (2018) proposed to approximate the effective wind speed within the plume from the 10 m wind by applying a multiplier in the range of 1.3–1.5. Therefore, we decided to use a multiplier of 1.4 for convenience. This empirical relationship accounts, e.g., for plume rise and mixing into altitudes with larger wind speeds. For the present, we consider this approximation adequate for this first study, but we recognize that uncertainties resulting from our (see next section) resulting from this estimate of the effective wind speed's normal may be reduced in the future by improved wind knowledge. However, in this study the focus is on demonstrating the benefits of simultaneous NO_2 and XCO_2 measurements rather than on most accurate flux estimates.

Additionally, it shall be noted that the plume cross-sectional flux (Eq. 2) is only a good approximation for the actual source emission under steady state (temporally invariant) conditions for wind speeds greater than about 2 m/s (Varon et al., 2018) when advection dominates over diffusion (Sharan et al., 1996). Changes in wind direction, wind speed, or atmospheric stability in the time span between emission and observation may result in differences between the plume cross-sectional flux and the source flux. Temporal variations in the source emissions of course also result in (temporally delayed) variations of the plume cross-sectional flux, which is always only a snap shot and must not be confused with, e.g., the annual average, even though given in the same units. In case of chemically active species (such as NO_2), also chemical processes along the plume path would have to be considered in order to compute source emissions from plume cross-sectional fluxes.

2.6 Uncertainty propagation

In order to estimate the uncertainty of the CO_2 plume cross-sectional flux (F_{CO_2}, Eq. 2), we propagate the uncertainties of the FWHM (a_4), the amplitude (a_7), and the wind speed normal (v_e) by assuming uncorrelated errors. The uncertainties of the FWHM and the amplitude result from the maximum likelihood fitting method propagating the uncertainties of the individual XCO_2 and NO_2 soundings as reported in the data products. The uncertainties of the wind components are read from the ECMWF ERA5 data archive resulting in total wind speed uncertainties ranging from 0.18 m/s to 0.33 m/s for the analyzed scenarios. Additionally, we assume that the manual adjustment of the wind direction is accurate by $\pm 10°$. These uncertainties propagate into the uncertainty of the wind speed normal. Varon et al. (2018) estimated that computing the effective wind speed from the 10 m wind introduces an additional uncertainty of 8-12%. However, we analyze scenes scenarios with larger plume structures and probably also larger variations of the injection heights which we consider by enhancing this error component to 20% for convenience. Uncertainties in the number of dry air particles are neglected as they are much smaller compared to, e.g., the wind speed uncertainty. As mentioned earlier, the assumption of constant meteorological conditions might not be valid in regions with large variations of the surface elevation or wind conditions within the plume's cross-section, which may result in an underestimation of the total cross-sectional flux uncertainty in such cases.

2.7 Plume detection and scenario selection

We use a semi-automatic method to select potentially interesting targets. In a first step, all co-locations of OCO-2 and S5P are computed similarly as described in section 2.3 but based on a coarser high resolution grid ($0.01° \times 0.01°$) to improve the computational efficiency. We shift a 30 s (~200 km) search window in time steps of 0.25 s (~2 km) over the time series of co-locations. Only those time steps are further considered which have at least 100 co-locations without data gaps exceeding 3 s (~20 km) within the search window. In the next step, we perform a least squares fit of the co-located XCO_2 and NO_2 data with a Gaussian vector function. This fitting function corresponds to Eq. 1 but with independent FWHM for XCO_2 and NO_2 and centered within the search window (a_3 and a_8 set to zero), which improves the convergence rate. Only those time steps are

Table 1. Summary of cross-sectional flux results including uncertainty contributions (1σ) and comparison with emission data bases EDGAR and ODIAC or GFED in the case of the Australian wildfires. The ODIAC values in brackets represent ODIAC emissions of 2016 and the month of the overpass in the same grid boxes as summed up for 2012. Note that the cross-sectional flux results correspond to the instantaneous time of the overpass' whilst EDGAR and ODIAC emissions are annual or monthly averages; GFED emissions correspond to six hourly averages (see Sec. 2.4). The uncertainty estimate comprises the total uncertainty and the uncertainties introduced by the ECMWF wind uncertainty, the uncertainty of the wind direction (10°), use of the 10 m wind (20%), the XCO_2 precision as reported in the data product, and the NO_2 precision as reported in the data product. All values are in units of $MtCO_2$/a.

Emission source	Cross-sect. flux	Cross-sectional flux uncertainty						EDGAR	ODIAC/ GFED*
		Total	ECMWF	Angle	10 m	XCO_2	NO_2		
Moscow	76	33	4	29	15	5	1	195	102 (88)
Lipetsk	69	50	5	48	14	1	0	23	4 (4)
Baghdad	95	36	3	30	19	6	1	22	13 (12)
Medupi and Matimba	31	7	3	2	6	2	0	0	24 (26)
Australian wildfires*	153	40	5	24	31	8	5	0	52
Nanjing	120	27	10	5	24	6	1	164	89 (96)

further considered fulfilling the following criteria: the fit converged, the NO_2 amplitude exceeds 10^{15}- molec./cm^2, the XCO_2 and NO_2 FWHM (a_c and a_n, respectively) do not exceed the half width of the search window ($a_c, a_n \leq 15\,s$) and do not differ by more than their average ($|a_c - a_n| \leq (a_c + a_n)/2$), the XCO_2 and NO_2 amplitudes are at least two times larger than their uncertainties and larger than the maximum variations of the backgrounds. In the last step, we decided by manual inspection of the XCO_2 and NO_2 co-locations plus the surrounding NO_2 fields and ECMWF wind information if the scenario is a promising candidate for further flux analyses. Potential reasons to reject an automatically pre-selected ~~scene~~ scenario are, e.g., too low wind speed, wind direction nearly parallel to OCO-2 orbit, unclear source attribution, or poor fit quality. In total we manually selected about 20 promising ~~scenes~~ scenarios in the time period ~~03~~01/2018 to 08/2018, of which we show 6 examples here.

3 Results

From the time period of ~~03~~01/2018 to 08/2018, we selected the following scenarios as examples for flux analyses based on co-located XCO_2 and NO_2 observations.

3.1 Moscow

Fig. 1a shows the NO_2 enhancement in ~~Moscow's city plume~~ the city plume of Moscow (approx. 12.4 million inhabitants) as retrieved from S5P overlayed by OCO-2's XCO_2 measurements. The NO_2 enhancement is clearly visible also in the plume's cross-section along OCO-2's ground track (Fig. 1c). Due to the larger relative noise of the XCO_2 retrievals, the XCO_2 enhancement is less obvious but still visible (Fig. 1c). The Gaussian fit of the enhancements is excellent for NO_2 and rea-

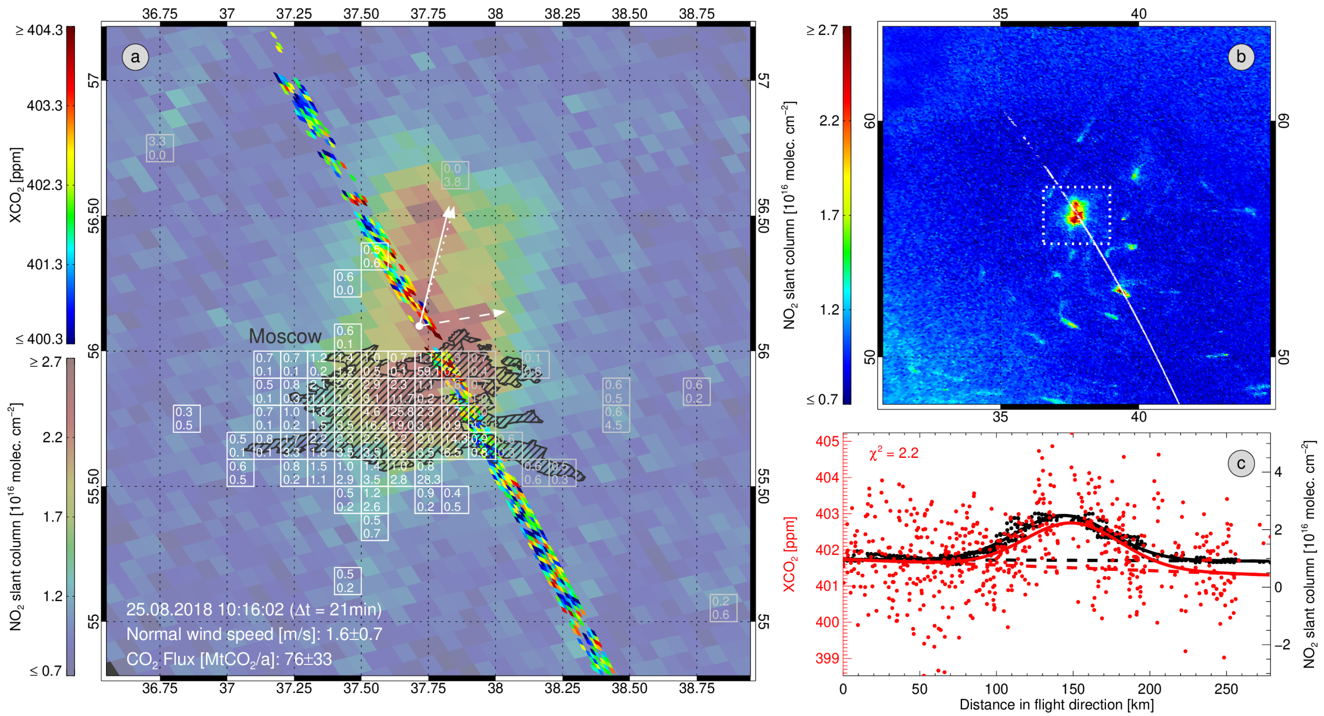

Figure 1. Moscow on August 25, 2018. **a)** S5P NO_2 slant column (background) overlayed by OCO-2 XCO_2 (foreground). Gray and white 0.1° boxes show EDGAR (bottom) and ODIAC (top) 2012 annual emissions with either EDGAR or ODIAC being larger than 0.5 $MtCO_2$/a. The white arrows show the direction of the 10 m wind as read from ECMWF (dotted), manually corrected to (subjectively) best match the NO_2 plume (solid), and normal to the OCO-2 orbit (dashed). Effective wind speed normal to the OCO-2 orbit, estimated cross-sectional CO_2 flux, time of OCO-2 overpass, and time difference between OCO-2 and S5P overpass are also listed. The hatched area corresponds to the urban area (World Urban Areas dataset, Geoportal of the University of California, *https://apps.gis.ucla.edu/geodata/dataset/world_urban_areas*). **b)** Larger section of the S5P NO_2 slant columns including the OCO-2 orbit and the bounding box of sub-figure a). **c)** OCO-2 XCO_2 values (red) and co-located S5P NO_2 slant columns (black) within the plume's cross-section in OCO-2 flight direction.

sonable ($\chi^2 = 2.2$) for XCO_2. There ~~is only a small adjustment needed~~ was nearly no adjustment needed (1°) to bring the ECMWF 10 m wind in good agreement with the NO_2 plume (Fig. 1a). The effective wind speed normal to the OCO-2 orbit amounts to 1.6±0.6 m/s which is a bit lower than optimal for reasonable flux estimates (Varon et al., 2018). The cross-sectional CO_2 flux amounts to 76±33 $MtCO_2$/a. This compares to 2012 average upwind emissions (white marked boxes in Fig. 1a) of 195 $MtCO_2$/a (EDGAR) and 102 $MtCO_2$/a (ODIAC). ODIAC's emission estimate for 08/2016 amounts to 88 $MtCO_2$/a. The NO_2 far field shows no indications for overlayed CO_2 plumes from other sources (Fig. 1b). The total flux uncertainty is dominated by the uncertainty of the wind direction followed by the uncertainty of the effective wind speed.

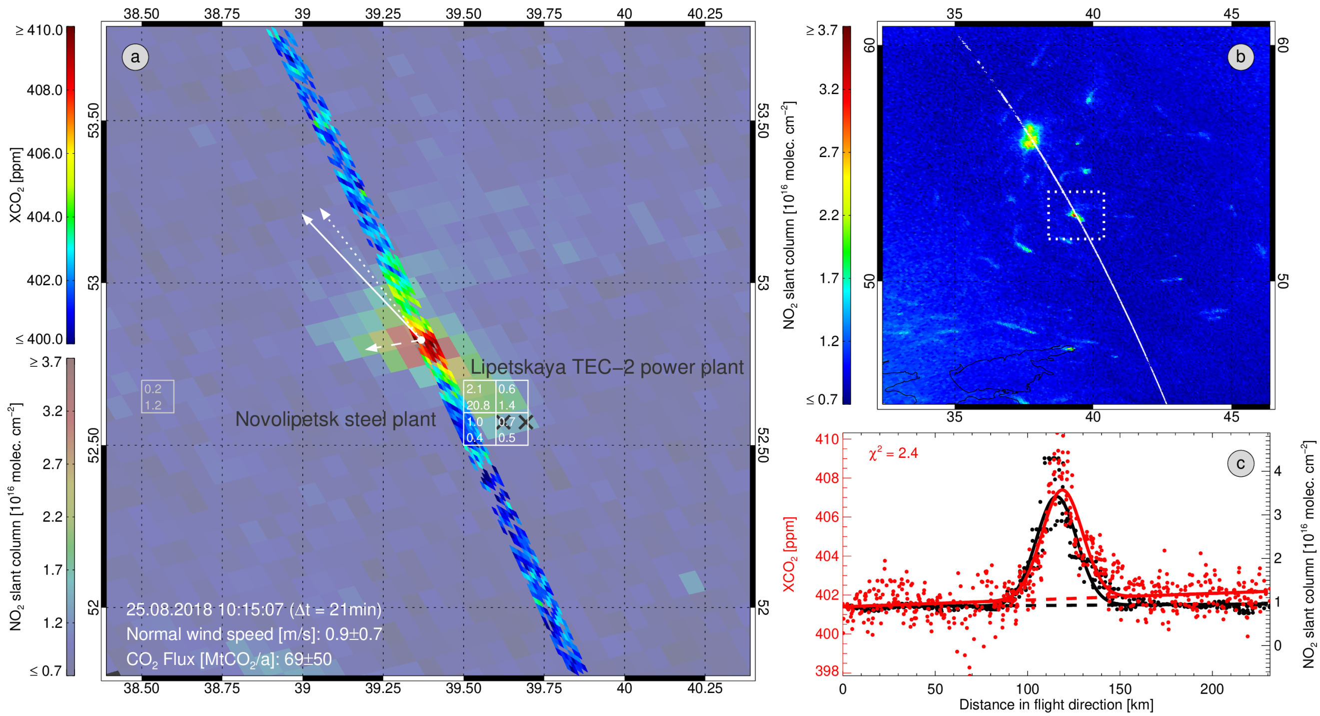

Figure 2. As Fig. 1 but for Lipetsk on August 25, 2018.

3.2 Lipetsk

Fig. 2a shows the surrounding of Lipetsk ~~with~~ (approx. 0.5 million inhabitants) with, among other industries, the Novolipetsk steel plant and the Lipetskaya TEC-2 gas-fired power plant (515MW) only one minute (~~-~~~400 km) apart from Moscow along OCO-2's flight track (see also Fig. 1b). The cross-sectional NO_2 and XCO_2 enhancements clearly stand out of the noise of the data (Fig. 2c) and the Gaussian function fits the XCO_2 data reasonably well ($\chi^2 = 2.4$). We applied ~~only~~ a small correction of 5° to the ECMWF wind direction. However, as the wind direction is similar to OCO-2's flight direction, the normal effective wind speed is unfavorably low (0.9±0.7 m/s) which makes the cross-sectional flux estimates (69±50 $MtCO_2$/a) less reliable and highly uncertain. The by far ~~larges~~ largest uncertainty contribution comes from the uncertainty of the wind direction. The 2012 average EDGAR and ODIAC upwind emissions (white marked boxes in Fig. 2a) are 23 $MtCO_2$/a and 4 $MtCO_2$/a (same for 08/2016), respectively, but the NO_2 far field shows no indications for overlayed CO_2 plumes from other sources (Fig. 2b).

3.3 Baghdad

Fig. 3a shows the S5P NO_2 slant columns overlayed by OCO-2 XCO_2 data in a surrounding of Baghdad ~~-~~(approx. 5.4 million inhabitants). Enhanced values are clearly visible in the cross-section of the NO_2 plume and less obviously visible also in the XCO_2 data (Fig. 3c). The XCO_2 enhancement is well fitted ($\chi^2 = 1.0$) by the Gaussian fitting function. The manually

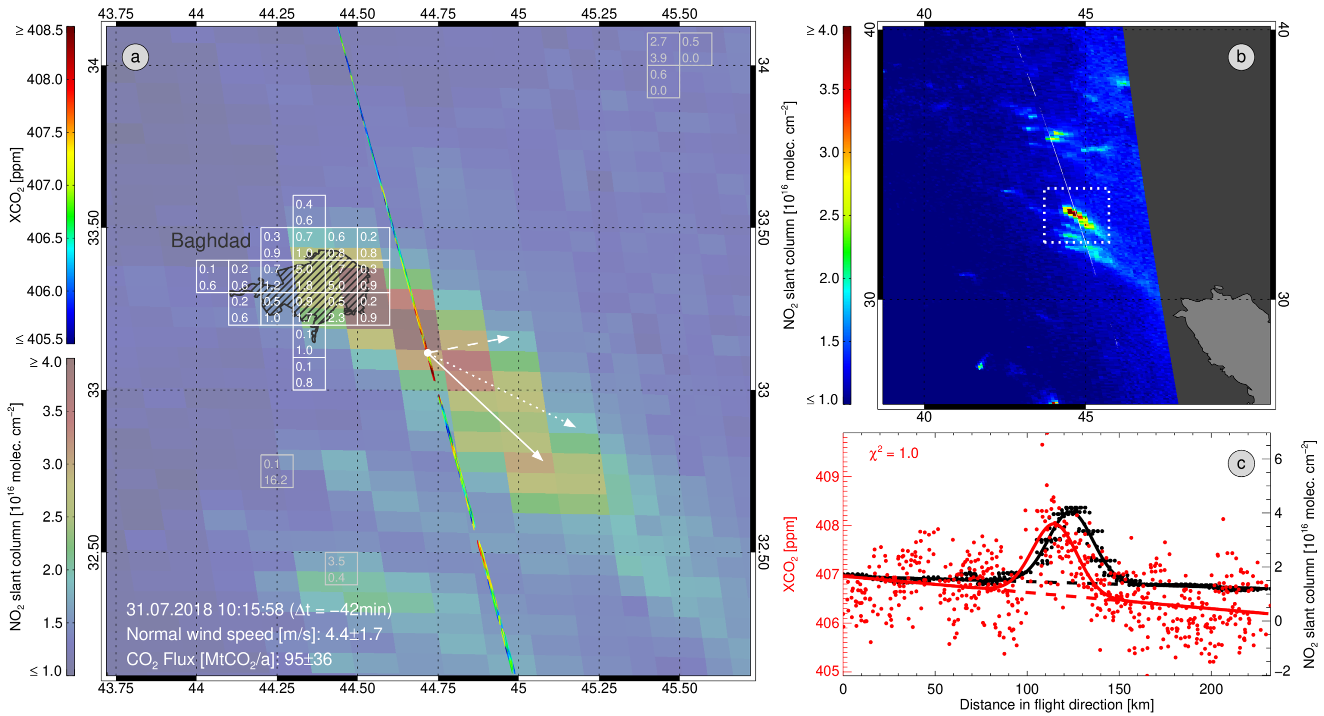

Figure 3. As Fig. 1 but for Baghdad on July 31, 2018.

adjusted wind direction ~~is similar to~~ deviates by 17° from the ECMWF wind direction and the normal wind speed amounts to 4.4±1.7 m/s. From the XCO_2 enhancement and the normal wind speed, we compute the cross-sectional CO_2 flux to be 95±36 $MtCO_2$/a. This compares to an upwind source of 22 $MtCO_2$/a or 13 $MtCO_2$/a (12 $MtCO_2$/a for 07/2016) of EDGAR or ODIAC, respectively. The flux uncertainty is dominated by the uncertainty of the wind direction and the uncertainty of the effective wind speed. The NO_2 far field shows no indications for overlayed CO_2 plumes from other sources (Fig. 3b).

3.4 Medupi and Matimba power plants

The Medupi (4764MW) and Matimba (3990MW) coal-fired power plants lie close to each other in South Africa about 300 km north of Johannesburg. Their NO_2 plume is shown in Fig. 4a overlayed by OCO_2 XCO_2 measurements. NO_2 measurements in the larger surrounding do not suggest any additional nearby upwind sources (Fig. 4b). The cross-sectional NO_2 values show a clear elevation within the plume which is less obvious for XCO_2 having larger relative scatter especially south of the plume. Nevertheless, the Gaussian function fits the XCO_2 values reasonably well ($\chi^2 = 1.4$). The wind direction (corrected by 13°) is nearly perpendicular to the OCO-2 orbit and the effective normal wind speed is 2.6±0.6 m/s. The cross-sectional CO_2 flux amounts to 31±7 $MtCO_2$/a which is consistent with ODIAC 2012 emissions of 24 $MtCO_2$/a and ODIAC 07/2016 emissions of 26 $MtCO_2$/a but EDGAR does not have significant emissions in this area. It shall be noted that the Medupi power plant started operation in 2015 with limited capacity and that it still has not reached its nominal capacity. Therefore, it is no surprise that

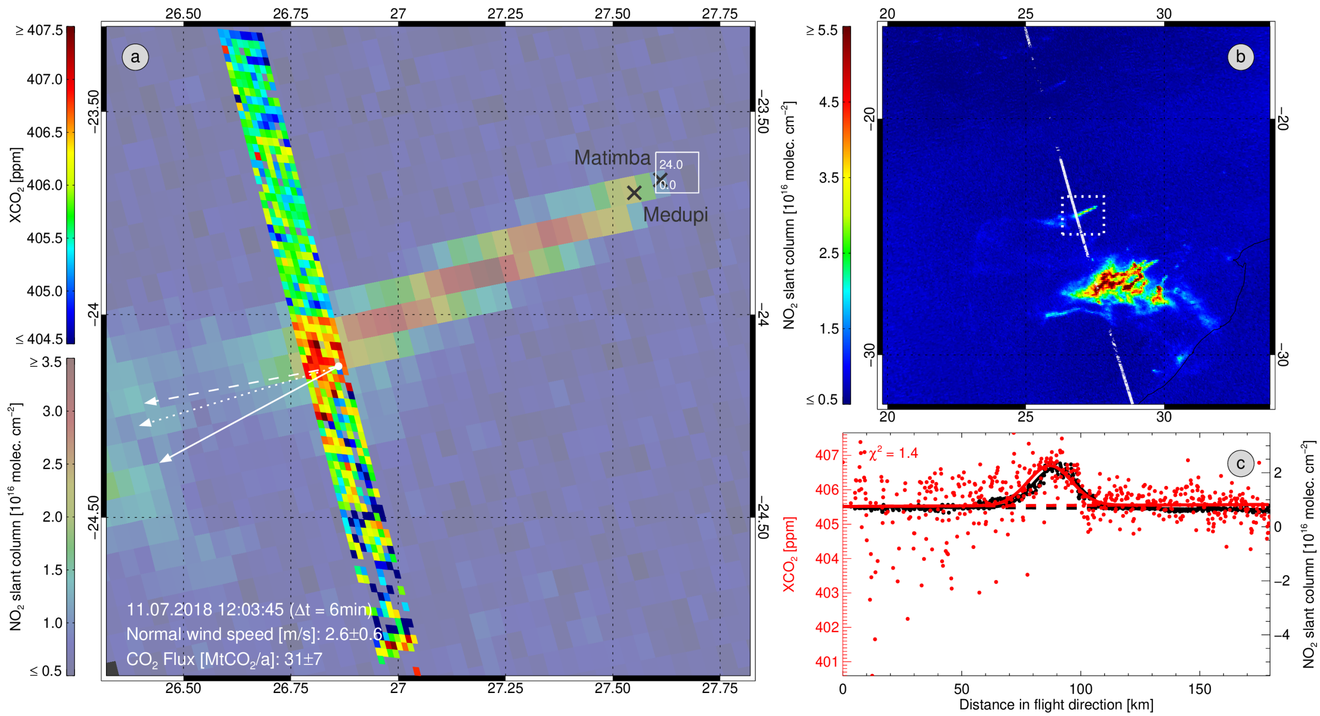

Figure 4. As Fig. 1 but for the Medupi and Matimba power plants in South Africa on July 11, 2018.

the Medupi power station is not included in either EDGAR or ODIAC 2012 data. The flux uncertainty is dominated by the uncertainty of the effective wind speed.

3.5 Australian wildfires

Fig. 5a shows the NO_2 plumes of two Australian wildfires on 05.05.2018 overlayed by an OCO-2 orbit of XCO_2 measurements. Enhanced NO_2 and XCO_2 values are clearly visible within the plume's cross-section (Fig. 5b). The NO_2 (and less obvious also the XCO_2) cross-section has two maxima ~~. The~~ which cannot be accounted for by the Gaussian fitting function~~cannot account for this, which is , however,~~. However, this is not reflected in the ~~overall good~~ good XCO_2 fit quality ($\chi^2 = 0.6$), but should be taken into account when valuing the results. We applied ~~only~~ a small manual correction of 7° to the wind direction and the effective wind speed normal to the OCO-2 orbit is 6.7±1.7 m/s. For the snapshot of the ~~overflight~~overpass, we computed a cross-sectional CO_2 flux of 153±40 $MtCO_2$/a. Its uncertainty is driven by the uncertainty of the effective wind speed and wind direction. As the shown plumes originate from wildfires, EDGAR and ODIAC do not include their emissions. However, GFED has average emissions of 52 $MtCO_2$/a within the six hours period 0h–6h UTC including the time of the overpass (5h UTC). The maximum GFED emissions are approximately at the position of the largest NO_2 concentrations. Fig. 5c shows no indications, that additional upwind sources may explain the discrepancy between our cross-sectional flux estimate and GFED.

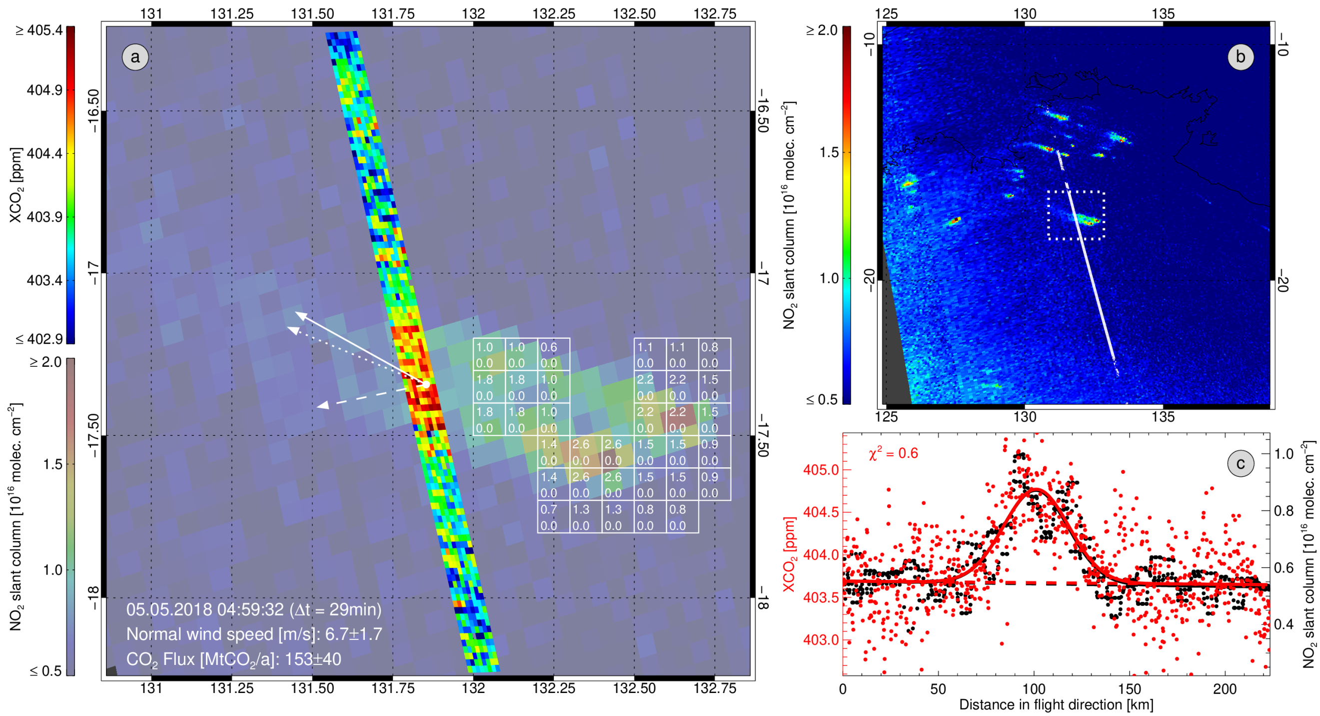

Figure 5. As Fig. 1 but for Australian wildfires on May 5, 2018. The ODIAC emission data (top number) have been replaced by GFED emissions for the time of the OCO-2 overpass.

3.6 Nanjing

Fig. 6a shows the NO_2 slant columns in the surrounding of Nanjing (approx. 5.8 million inhabitants) overlayed by OCO-2 XCO_2 measurements. The cross-section along the OCO-2 orbit shows strong XCO_2 and and NO_2 plume signals distinctively above the noise level which are well fitted with the Gaussian fitting function ($\chi^2 = 0.6$). The ECMWF wind direction is not far from being rectangular to the OCO-2 orbit and we applied ~~only~~ a moderate manual correction of 11°. The effective normal wind speed is 2.2±0.5 m/s. This results in a cross-sectional flux estimate of 120±27 $MtCO_2$/a which lies in between the upwind emissions of EDGAR (163 $MtCO_2$/a) and ODIAC (89 $MtCO_2$/a for 2012, 96 $MtCO_2$/a for 03/2016). Fig. 6b does not indicate additional major remote upwind sources. The uncertainty of the cross-sectional flux estimate is dominated by the uncertainty of the effective wind speed.

4 Discussion and conclusions

Based on six case studies (Moscow, Russia; Lipetsk, Russia; Baghdad, Iraq; Medupi and Matimba power plants, South Africa; Australian wildfires; and Nanjing, China), we demonstrated the usefulness of simultaneous satellite observations of NO_2 and the column-average dry-air mole fraction of CO_2 (XCO_2). For this purpose, we analyzed co-located regional enhancements of

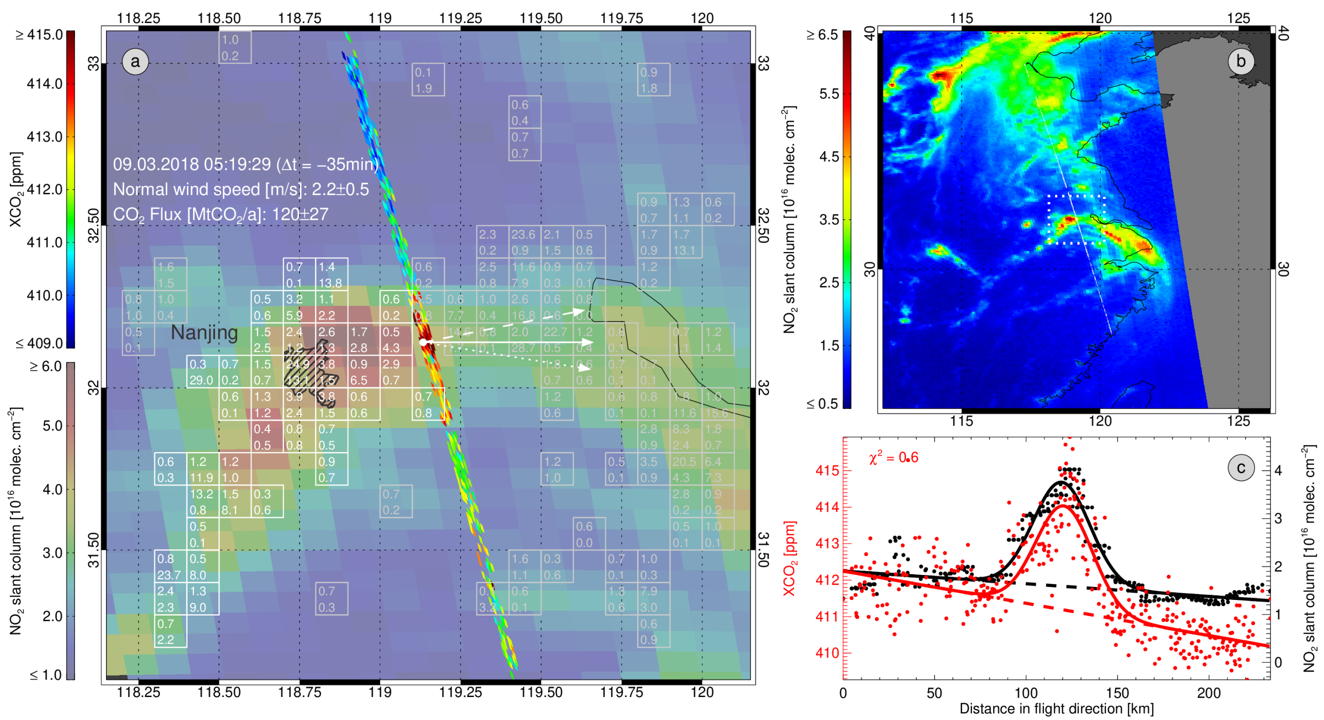

Figure 6. As Fig. 1 but for Nanjing on March 9, 2018.

XCO_2 observed by OCO-2 and NO_2 ~~observed by~~ from S5P and estimated the CO_2 plume's cross-sectional fluxes. For atmospheric standard conditions, we approximated as a rule of thumb, that a Gaussian enhancement of 1 ppm with a width of 1 km at a wind speed (normal to the cross-section) of 1 m/s corresponds to a plume cross-sectional flux of roughly 0.53 $MtCO_2$/a.

For Moscow, we derived a cross-sectional flux of 76±33 $MtCO_2$/a which agrees (within its uncertainty) with ODIAC 2012 emissions of 102 $MtCO_2$/a (88 $MtCO_2$/a for 08/2016) but not with EDGAR emissions of 195 $MtCO_2$/a. The cross-sectional flux estimate of Lipetsk with the Novolipetsk steel plant and the Lipetskaya TEC-2 power plant is 69±50 $MtCO_2$/a. Within its uncertainty, this estimate agrees with EDGAR emissions of 23 $MtCO_2$/a but not with ODIAC emissions of 4 $MtCO_2$/a. However, the uncertainty of the estimate is large due to a wind direction with an acute angle relative to the OCO-2 orbit which also results in a low effective normal wind speed. This can serve as an example for low wind speeds being favorable for plume detection but not necessarily for flux quantification. In the case of Baghdad, we derived a cross-sectional flux of 95±36 $MtCO_2$/a for the time of the overpass which is considerably larger than the annual average EDAGR (22 $MtCO_2$/a) and ODIAC (13 $MtCO_2$/a for 2012, 12 $MtCO_2$/a for 07/2016) emissions of 2012. The wind conditions were relatively good and S5P NO_2 measurements do not suggest an overlaying significant upwind source. In this context, it is interesting to note that Georgoulias et al. (2019) found a strongly increasing trend (17.0±0.8%/a in the period 04/1996–09/2017) for the tropospheric NO_2 concentrations in Baghdad (and a decreasing trend of -2.2±0.7%/a for Iraq) hinting at strongly increasing CO_2 emissions in Baghdad since 2012. The cross-sectional flux of the plume of the Medupi and Matimba power plants have been estimated to 31±7 $MtCO_2$/a which agrees (within its uncertainty) with ODIAC (24 $MtCO_2$/a for 2012, 26 $MtCO_2$/a for 07/2016) but not with EDGAR (no significant emission). ~~For~~ Nassar et al. (2017) also estimated the emissions from the Matimba power plant (but not Medupi) using OCO-2 XCO_2 v7 data. For a direct overpass in 2014 and a close flyby (∼7 km away) in 2016 they found fluxes, converted to annual values, of 12.1±3.9 $MtCO_2$/a and 12.3±1.2 $MtCO_2$/a, respectively. For the Australian wildfires, we estimated a plume cross-sectional flux of 153±40 $MtCO_2$/a which is about three times larger than the GFED estimate (52 $MtCO_2$/a) for a six hours average ending approximately at the time of the OCO-2 ~~overflight~~overpass. Unfavorable wind conditions or a strong overlaying upwind source can be excluded as reason for the discrepancy. The same is true for the fact that a double-plume structure has been fitted with a Gaussian function. However, it shall be noted that GFED's emission estimate for the same time interval but one day before the OCO-2 overpass amounts to 252 $MtCO_2$/a. For the Nanjing ~~scene~~scenario, we derived a cross-sectional flux of 120±27 $MtCO_2$/a which lies in between ODIAC (89 $MtCO_2$/a for 2012, 96 $MtCO_2$/a for 03/2016) and EDGAR (164 $MtCO_2$/a). However, the scene includes a larger area of ~~overlayed~~ overlaying sources, making source attribution difficult.

The total uncertainty of the derived plume cross-sectional fluxes ranges from 7 $MtCO_2$/a to 50 $MtCO_2$/a or in relative measures from 23% to 72%. The total uncertainty is always dominated by an uncertainty contribution related to meteorology. Specifically, the (manually adjusted) wind direction or the computation of the effective wind speed from the 10 m wind contribute most to the total uncertainty. The noise of the XCO_2 retrievals contributes only with 1 $MtCO_2$/a to 8 $MtCO_2$/a to the total error and the noise of the NO_2 retrievals contributes on average even three times less.

It is unlikely, that the observed XCO_2 enhancements are dominated by uncorrected enhancements due to co-emitted aerosols because the OCO-2 retrieval algorithm accounts for light scattering at optically thin aerosol layers and filters scenes with stronger aerosol contamination. Additionally, Bovensmann et al. (2010) estimated for the proposed CarbonSat (Carbon Monitoring Satellite) instrument that neglecting co-emitted aerosols in power plant plumes results in errors between 0.2 $MtCO_2$/a and 2.5 $MtCO_2$/a which is small compared with the derived cross-sectional fluxes and their total uncertainties (Tab. 1). Aerosols can also effect the S5P NO_2 slant columns which is, however, less important for our work because we derive only the plume width and direction from the NO_2 observations.

It shall be noted that differences of the cross-sectional flux estimates and the emission data bases are not necessarily coming from inaccuracies of the satellite retrievals or the emission data bases. Our estimates are valid only for the time of the overpass while the emission data bases give annual or monthly averages. Velazco et al. (2011) illustrated, that power plants can have substantial annual and day-to-day variations. Additionally, the cross-sectional flux is only a good approximation for the source emission under meteorological steady state conditions with wind speeds greater than about 2 m/s (Varon et al., 2018).

For the analyzed scenarios, we observe rather large differences between the EDGAR and ODIAC emission inventories. However, note that only those grid boxes are shown (and summed up) in Fig. 1a–6a for which either EDGAR or ODIAC emissions are larger than 0.5~~/~~ $MtCO_2$/a. This means, a smoother distribution of emissions may be misinterpreted as less emissions, if a significant fraction of the total emission is located in grid boxes not exceeding the 0.5~~/~~ $MtCO_2$/a threshold. Additionally, it shall be noted that ODIAC emissions correspond to fossil fuel combustion and cement production only, while EDGAR includes also emissions from other sectors (e.g., agriculture, land use change, and waste).

NO_2 is co-emitted with CO_2 when fossil fuels are combusted at high temperatures and has a relatively short lifetime of the order of hours which makes it a suitable tracer for recently emitted CO_2. Despite less strict quality filtering is needed, plume enhancements of NO_2 columns near sources can be retrieved from satellites with much lower relative noise than this is the case for XCO_2. We take advantage of this these points by using NO_2 measurements to i) identify the source of the observed XCO_2 enhancements, ii) to exclude interference with potential additional remote upwind sources, iii) to manually adjust the wind direction, and iv) to put a constraint on the shape of the observed CO_2 plumes.

In principle, it is also be possible, to fit only the XCO_2 values without constraining the plume shape by NO_2. In this case, XCO_2 is used to derive the amplitude and FWHM of the enhancement. We repeated the flux estimation of all shown scenarios with such a setup and got consistent flux results but with an fluxes of 61±27 MtCO$_2$/a, 63±46 MtCO$_2$/a, 75±29 MtCO$_2$/a, 35±9 MtCO$_2$/a, 166±44 MtCO$_2$/a, and 119±28 MtCO$_2$/a for the Moscow, Lipetsk, Baghdad, Medupi/Matimba, Australian wildfires, and Nanjing scenario, respectively. The derived fluxes are consistent within their uncertainty with our main results shown in Tab. 1, but the uncertainty contribution due to the noise in the XCO_2 data increased by about 33% 34% from 4.7 MtCO$_2$/a to 6.3 MtCO$_2$/a on average.

Reuter et al. (2014) discussed that post ENVISAT post-ENVISAT missions such as OCO-2 would benefit from co-located measurements of co-emitted species from other satellites or ideally multi-species measurements from the same instrument. We demonstrated, that the analysis of small scale emissions in OCO-2 XCO_2 data indeed profits from simultaneous NO_2 observations of S5P as they allow to set the XCO_2 observations into context but also to constrain the plume structure. The uncertainties of the cross-sectional flux estimates due to meteorology and their agreement with the actual emissions might be improved in subsequent studies by making use of dedicated simulations with Lagrangian particle dispersion models with either known source positions (and injection heights) or source positions inferred from the NO_2 data.

However, we expect the largest room for improvements in satellite missions such as the planned European Copernicus anthropogenic CO_2 monitoring mission (CO2M) which will provide not only precise measurements with high spatial resolution but also imaging capabilities with a wider swath of simultaneous XCO_2 and NO_2 observations. Its imaging capabilities will reduce the uncertainty of the inferred emissions due to measurement noise simply because of the increased number of soundings. Additionally, simultaneous XCO_2 and NO_2 observations from the same platform will allow stricter constraints on the plume shape. More importantly, the meteorology related uncertainties will reduce (Varon et al., 2018) because deviations from steady state conditions can average out and are, therefore, less critical if the entire plume structure is sampled rather than only a cross-section.

Author contributions. M.R.: experimental set-up, data analysis, interpretation, writing the paper. M.B., O.S., S.K., H.B., J.P.B.: experimental set-up, interpretation, improving the paper. A.R.: interpretation, design and operation of the NO_2 satellite retrieval, improving the paper. C.W.O'D.: interpretation, design and operation of the XCO_2 satellite retrieval, improving the paper.

Competing interests. The authors declare that they have no conflict of interest.

Acknowledgements. This work was funded by the State and the University of Bremen. The OCO-2 XCO_2 data were produced by the OCO-2 project at the Jet Propulsion Laboratory, California Institute of Technology, and obtained from the OCO-2 data archive maintained at the NASA Goddard Earth Science Data and Information Services Center. This publication contains modified Copernicus Sentinel data (2018). S5P is an ESA mission implemented on behalf of the European Commission. The TROPOMI payload is a joint development by ESA and the Netherlands Space Office (NSO). The S5P ground-segment development has been funded by ESA and with national contributions from The Netherlands, Germany, and Belgium. ERA5 meteorological profiles have been obtained from the Copernicus Climate Change Service (C3S) operated by ECMWF. CO_2 emission data have been obtained from the EDGAR, ODIAC, and the GFED data bases.

References

Boersma, K., Eskes, H., Veefkind, J., Brinksma, E., Van Der A, R., Sneep, M., Van Den Oord, G., Levelt, P., Stammes, P., Gleason, J., et al.: Near-real time retrieval of tropospheric NO_2 from OMI, Atmospheric Chemistry and Physics, 7, 2103–2118, 2007.

Bovensmann, H., Burrows, J. P., Buchwitz, M., Frerick, J., Noël, S., Rozanov, V. V., Chance, K. V., and Goede, A.: SCIAMACHY – Mission Objectives and Measurement Modes, Journal of the Atmospheric Sciences, 56, 127–150, http://dx.doi.org/10.1175/1520-0469(1999)056<0127:SMOAMM>2.0.CO;2, 1999.

Bovensmann, H., Buchwitz, M., Burrows, J. P., Reuter, M., Krings, T., Gerilowski, K., Schneising, O., Heymann, J., Tretner, A., and Erzinger, J.: A remote sensing technique for global monitoring of power plant CO_2 emissions from space and related applications, Atmospheric Measurement Techniques, 3, 781–811, https://doi.org/10.5194/amt-3-781-2010, http://www.atmos-meas-tech.net/3/781/2010/, 2010.

Brunner, D., Kuhlmann, G., Marshall, J., Clément, V., Fuhrer, O., Broquet, G., Löscher, A., and Meijer, Y.: Accounting for the vertical distribution of emissions in atmospheric CO_2 simulations, Atmospheric Chemistry and Physics, 19, 4541–4559, 2019.

Buchwitz, M., Schneising, O., Reuter, M., Heymann, J., Krautwurst, S., Bovensmann, H., Burrows, J. P., Boesch, H., Parker, R. J., Somkuti, P., Detmers, R. G., Hasekamp, O. P., Aben, I., Butz, A., Frankenberg, C., and Turner, A. J.: Satellite-derived methane hotspot emission estimates using a fast data-driven method, Atmospheric Chemistry and Physics, 17, 5751–5774, https://doi.org/10.5194/acp-17-5751-2017, https://www.atmos-chem-phys.net/17/5751/2017/, 2017.

Burrows, J. P., Hölzle, E., Goede, A. P. H., Visser, H., and Fricke, W.: SCIAMACHY – Scanning Imaging Absorption Spectrometer for Atmospheric Chartography, Acta Astronautica, 35, 445–451, 1995.

Ciais, P., Dolman, A. J., Bombelli, A., Duren, R., Peregon, A., Rayner, P. J., Miller, C., Gobron, N., Kinderman, G., Marland, G., Gruber, N., Chevallier, F., Andres, R. J., Balsamo, G., Bopp, L., Bréon, F.-M., Broquet, G., Dargaville, R., Battin, T. J., Borges, A., Bovensmann, H., Buchwitz, M., Butler, J., Canadell, J. G., Cook, R. B., DeFries, R., Engelen, R., Gurney, K. R., Heinze, C., Heimann, M., Held, A., Henry, M., Law, B., Luyssaert, S., Miller, J., Moriyama, T., Moulin, C., Myneni, R. B., Nussli, C., Obersteiner, M., Ojima, D., Pan, Y., Paris, J.-D., Piao, S. L., Poulter, B., Plummer, S., Quegan, S., Raymond, P., Reichstein, M., Rivier, L., Sabine, C., Schimel, D., Tarasova, O., Valentini, R., Wang, R., van der Werf, G., Wickland, D., Williams, M., and Zehner, C.: Current systematic carbon-cycle observations and the need for implementing a policy-relevant carbon observing system, Biogeosciences, 11, 3547–3602, https://doi.org/10.5194/bg-11-3547-2014, http://www.biogeosciences.net/11/3547/2014/, 2014.

Crisp, D., Atlas, R. M., Bréon, F.-M., Brown, L. R., Burrows, J. P., Ciais, P., Connor, B. J., Doney, S. C., Fung, I. Y., Jacob, D. J., Miller, C. E., O'Brien, D., Pawson, S., Randerson, J. T., Rayner, P., Salawitch, R. S., Sander, S. P., Sen, B., Stephens, G. L., Tans, P. P., Toon, G. C., Wennberg, P. O., Wofsy, S. C., Yung, Y. L., Kuang, Z., Chudasama, B., Sprague, G., Weiss, P., Pollock, R., Kenyon, D., and Schroll, S.: The Orbiting Carbon Observatory (OCO) mission, Advances in Space Research, 34, 700–709, 2004.

Georgoulias, A. K., van der A, R. J., Stammes, P., Boersma, K. F., and Eskes, H. J.: Trends and trend reversal detection in 2 decades of tropospheric NO_2 satellite observations, Atmospheric Chemistry and Physics, 19, 6269–6294, https://doi.org/10.5194/acp-19-6269-2019, https://www.atmos-chem-phys.net/19/6269/2019/, 2019.

Heymann, J., Reuter, M., Buchwitz, M., Schneising, O., Bovensmann, H., Burrows, J., Massart, S., Kaiser, J., and Crisp, D.: CO_2 emission of Indonesian fires in 2015 estimated from satellite-derived atmospheric CO_2 concentrations, Geophysical Research Letters, 44, 1537–1544, 2017.

Kiel, M., O'Dell, C. W., Fisher, B., Eldering, A., Nassar, R., MacDonald, C. G., and Wennberg, P. O.: How bias correction goes wrong: measurement of XCO_2 affected by erroneous surface pressure estimates, Atmospheric Measurement Techniques, 12, 2241–2259, https://doi.org/10.5194/amt-12-2241-2019, https://www.atmos-meas-tech.net/12/2241/2019/, 2019.

Kort, E. A., Frankenberg, C., Miller, C. E., and Oda, T.: Space-based observations of megacity carbon dioxide, Geophysical Research Letters, 39, https://doi.org/10.1029/2012GL052738, 2012.

Krings, T., Gerilowski, K., Buchwitz, M., Reuter, M., Tretner, A., Erzinger, J., Heinze, D., Pflüger, U., Burrows, J. P., and Bovensmann, H.: MAMAP - a new spectrometer system for column-averaged methane and carbon dioxide observations from aircraft: retrieval algorithm and first inversions for point source emission rates, Atmospheric Measurement Techniques, 4, 1735–1758, https://doi.org/10.5194/amt-4-1735-2011, https://www.atmos-meas-tech.net/4/1735/2011/, 2011.

Krings, T., Neininger, B., Gerilowski, K., Krautwurst, S., Buchwitz, M., Burrows, J. P., Lindemann, C., Ruhtz, T., Schüttemeyer, D., and Bovensmann, H.: Airborne remote sensing and in situ measurements of atmospheric CO_2 to quantify point source emissions, Atmospheric Measurement Techniques, 11, 721–739, https://doi.org/10.5194/amt-11-721-2018, https://www.atmos-meas-tech.net/11/721/2018/, 2018.

Kuze, A., Suto, H., Nakajima, M., and Hamazaki, T.: Thermal and near infrared sensor for carbon observation Fourier-transform spectrometer on the Greenhouse Gases Observing Satellite for greenhouse gases monitoring, Applied Optics, 48, 6716, https://doi.org/10.1364/AO.48.006716, http://dx.doi.org/10.1364/AO.48.006716, 2009.

Nassar, R., Hill, T. G., McLinden, C. A., Wunch, D., Jones, D., and Crisp, D.: Quantifying CO_2 emissions from individual power plants from space, Geophysical Research Letters, 44, 2017.

Oda, T., Maksyutov, S., and Andres, R. J.: The Open-source Data Inventory for Anthropogenic CO_2, version 2016 (ODIAC2016): a global monthly fossil fuel CO_2 gridded emissions data product for tracer transport simulations and surface flux inversions, Earth System Science Data, 10, 87–107, https://doi.org/10.5194/essd-10-87-2018, https://www.earth-syst-sci-data.net/10/87/2018/, 2018.

O'Dell, C. W., Eldering, A., Wennberg, P. O., Crisp, D., Gunson, M. R., Fisher, B., Frankenberg, C., Kiel, M., Lindqvist, H., Mandrake, L., Merrelli, A., Natraj, V., Nelson, R. R., Osterman, G. B., Payne, V. H., Taylor, T. E., Wunch, D., Drouin, B. J., Oyafuso, F., Chang, A., McDuffie, J., Smyth, M., Baker, D. F., Basu, S., Chevallier, F., Crowell, S. M. R., Feng, L., Palmer, P. I., Dubey, M., García, O. E., Griffith, D. W. T., Hase, F., Iraci, L. T., Kivi, R., Morino, I., Notholt, J., Ohyama, H., Petri, C., Roehl, C. M., Sha, M. K., Strong, K., Sussmann, R., Te, Y., Uchino, O., and Velazco, V. A.: Improved retrievals of carbon dioxide from Orbiting Carbon Observatory-2 with the version 8 ACOS algorithm, Atmospheric Measurement Techniques, 11, 6539–6576, https://doi.org/10.5194/amt-11-6539-2018, https://www.atmos-meas-tech.net/11/6539/2018/, 2018.

Pinty, B., Janssens-Maenhout, G., M., D., Zunker, H., Brunhes, T., Ciais, P., Denier van der Gon, D. Dee, H., Dolman, H., M., D., Engelen, R., Heimann, M., Holmlund, K., Husband, R., Kentarchos, A., Meijer, Y., Palmer, P., and Scholze, M.: An Operational Anthropogenic CO_2 Emissions Monitoring & Verification Support capacity - Baseline Requirements, Model Components and Functional Architecture, European Commission Joint Research Centre, EUR 28736 EN, https://doi.org/10.2760/39384, http://copernicus.eu/sites/default/files/library/Report_Copernicus_CO2_Monitoring_TaskForce_Nov2017.pdf, 2017.

Reuter, M., Buchwitz, M., Hilboll, A., Richter, A., Schneising, O., Hilker, M., Heymann, J., Bovensmann, H., and Burrows, J.: Decreasing emissions of NO_x relative to CO_2 in East Asia inferred from satellite observations, Nature Geoscience, 7, 792, 2014.

Reuter, M., Buchwitz, M., Schneising, O., Noël, S., Bovensmann, H., and Burrows, J. P.: A fast atmospheric trace gas retrieval for hyperspectral instruments approximating multiple scattering - Part 2: application to XCO_2 retrievals from OCO-2, Remote Sensing, 9, https://doi.org/10.3390/rs9111102, http://www.mdpi.com/2072-4292/9/11/1102, 2017.

Richter, A., Burrows, J. P., Nüß, H., Granier, C., and Niemeier, U.: Increase in tropospheric nitrogen dioxide over China observed from space, Nature, 437, 129–132, https://doi.org/10.1038/nature04092, 2005.

Richter, A., Begoin, M., Hilboll, A., and Burrows, J.: An improved NO_2 retrieval for the GOME-2 satellite instrument, Atmospheric Measurement Techniques, 4, 1147–1159, 2011.

Rockström, J., Gaffney, O., Rogelj, J., Meinshausen, M., Nakicenovic, N., and Schellnhuber, H. J.: A roadmap for rapid decarbonization, Science, 355, 1269–1271, 2017.

Schneising, O., Heymann, J., Buchwitz, M., Reuter, M., Bovensmann, H., and Burrows, J. P.: Anthropogenic carbon dioxide source areas observed from space: assessment of regional enhancements and trends, Atmospheric Chemistry and Physics, 13, 2445–2454, https://doi.org/10.5194/acp-13-2445-2013, http://www.atmos-chem-phys.net/13/2445/2013/, 2013.

Sharan, M., Yadav, A. K., Singh, M., Agarwal, P., and Nigam, S.: A mathematical model for the dispersion of air pollutants in low wind conditions, Atmospheric Environment, 30, 1209–1220, 1996.

Varon, D. J., Jacob, D. J., McKeever, J., Jervis, D., Durak, B. O. A., Xia, Y., and Huang, Y.: Quantifying methane point sources from fine-scale satellite observations of atmospheric methane plumes, Atmospheric Measurement Techniques, 11, 5673–5686, https://doi.org/10.5194/amt-11-5673-2018, https://www.atmos-meas-tech.net/11/5673/2018/, 2018.

Veefkind, J., Aben, I., McMullan, K., Förster, H., De Vries, J., Otter, G., Claas, J., Eskes, H., De Haan, J., Kleipool, Q., et al.: TROPOMI on the ESA Sentinel-5 Precursor: A GMES mission for global observations of the atmospheric composition for climate, air quality and ozone layer applications, Remote Sensing of Environment, 120, 70–83, 2012.

Velazco, V. A., Buchwitz, M., Bovensmann, H., Reuter, M., Schneising, O., Heymann, J., Krings, T., Gerilowski, K., and Burrows, J. P.: Towards space based verification of CO_2 emissions from strong localized sources: fossil fuel power plant emissions as seen by a CarbonSat constellation, Atmospheric Measurement Techniques, 4, 2809–2822, https://doi.org/10.5194/amt-4-2809-2011, https://www.atmos-meas-tech.net/4/2809/2011/, 2011.